frontiers | Frontiers in Marine Science

ORIGINAL RESEARCH
published: 05 April 2022
doi: 10.3389/fmars.2022.820731

High-Resolution Reconstruction of Dissolved Oxygen Levels in the Baltic Sea With Bivalves – a Multi-Species Comparison (*Arctica islandica*, *Astarte borealis*, *Astarte elliptica*)

Bernd R. Schöne[1]*, *Xizhi Huang*[1], *Anne Jantschke*[1], *Regina Mertz-Kraus*[1] and *Michael L. Zettler*[2]

[1] Institute of Geosciences, University of Mainz, Mainz, Germany, [2] Biological Oceanography, Leibniz Institute for Baltic Sea Research Warnemünde, Rostock, Germany

OPEN ACCESS

Edited by:
Dongyan Liu,
East China Normal University, China

Reviewed by:
Kefu Yu,
Guangxi University, China
Yujue Wang,
East China Normal University, China

***Correspondence:**
Bernd R. Schöne
bernd.schoene@uni-mainz.de

Specialty section:
This article was submitted to Marine Ecosystem Ecology, a section of the journal Frontiers in Marine Science

Received: 23 November 2021
Accepted: 10 March 2022
Published: 05 April 2022

Citation:
Schöne BR, Huang X, Jantschke A, Mertz-Kraus R and Zettler ML (2022) High-Resolution Reconstruction of Dissolved Oxygen Levels in the Baltic Sea With Bivalves – a Multi-Species Comparison (Arctica islandica, Astarte borealis, Astarte elliptica). Front. Mar. Sci. 9:820731. doi: 10.3389/fmars.2022.820731

An increasing area of shallow-marine benthic habitats, specifically in the Baltic Sea, is affected by seasonal oxygen depletion. To place the current spread of oxygen deficiency into context and quantify the contribution of anthropogenic ecosystem perturbation to this development, high-resolution archives for the pre-instrumental era are needed. As recently demonstrated, shells of the bivalve mollusk, *Arctica islandica* fulfil this task with molar Mn/Ca_{shell} ratios as proxies for dissolved oxygen (DO) levels in the water column. Since the ocean quahog is inhomogeneously distributed in the Baltic Sea and may not be present in museum collections or found throughout sedimentary sequences, the present study evaluated whether two other common bivalves, *Astarte elliptica* and *Astarte borealis* can be used interchangeably or alternatively as proxy DO recorders. Once mathematically resampled and corrected for shell growth rate-related kinetic effects and (some) vital effects, Mn/Ca_{shell} data of all three species (age ten onward in *A. islandica*) were statistically significantly ($p < 0.0001$) linearly and inversely correlated to DO concentration in the free water column above seafloor ($r = -0.66$ to -0.75, corresponding to 43 to 56% explained variability). *A. elliptica* may provide slightly more precise DO data (1σ error of ±1.5 mL/L) than *A. islandica* or *A. borealis* (± 1.6 mL/L), but has a shorter lifespan. Both *Astarte* species show a stronger correlation with DO than *A. islandica*, because their biomineralization seems to be less severely hampered by oxygen and salinity stress. In turn, *A. islandica* grows faster resulting in less time-averaged data. During youth, the ocean quahog typically incorporates a disproportionately large amount of manganese into its shell, possibly because food intake occurs directly at the sediment-water interface where Mn-rich porewater diffuses out of the sediment. With increasing

age, however, *A. islandica* seems to generate a gradually stronger inhaling water current and takes in a larger proportion of water farther away from the fluffy layer. As demonstrated here, all three studied species can be used as DO archives, though species-specific limitations should be kept in mind.

Keywords: sclerochronology, bivalve mollusk, shell, hypoxia, manganese, dissolved oxygen proxy, multispecies comparison

1 INTRODUCTION

Severe oxygen deficiency endangers aquatic ecosystems potentially resulting in dead zones. When dissolved oxygen (DO) concentration falls below approx. 2.3 mg/L (≙ 1.6 mL/L or 72 µmol/L; Vaquer-Sunyer and Duarte, 2008; equivalent to approx. 30% DO saturation; Rabalais et al., 2010) – the transition from normoxic to hypoxic waters –, most invertebrates and fish can no longer properly respire (Herreid, 1980). As a consequence, diversity decreases, food webs collapse and biogeochemical cycles change, which in turn can further fuel oxygen depletion (Österblom et al., 2007), eventually until all free oxygen is consumed, and anoxic conditions and dead zones emerge.

As indicated by abundant dark grey and black shale deposits, widespread depletion or absence of DO near the seabed has been a common and recurring phenomenon during Earth history (Tyson and Pearson, 1991; Arthur and Sageman, 1994) and continues to do so. Since the beginning of the 20th century, oxygen-deficiency has significantly expanded and now also threatens nearshore coastal environments (Conley et al., 2009; Carstensen et al., 2014; Fennel and Testa, 2019). Despite extensive research – predominantly in the Baltic Sea, one of the largest marine low-oxygen settings – the mechanisms and ultimate causes of coastal hypoxia are still not well understood, but likely include anthropogenic eutrophication that propelled primary production and increased the flux of organic carbon to the seafloor (Conley et al., 2007; Carstensen et al., 2014). This deficit of knowledge is largely attributed to incomplete instrumental data and lack of suitable high-resolution archives. Whereas DO trends on time-scales of centuries and millennia can be reconstructed from sediment cores (Jokinen et al., 2018), annually and better resolved, temporally well-constrained archives are still scarce. Besides fish otoliths (Limburg et al., 2011) and foraminifera (Groeneveld and Filipsson, 2013), shells of the marine bivalve mollusk, *Arctica islandica* have recently been identified as interannually to seasonally resolved *in-situ* archives of oxygen deficiency with manganese-to-calcium molar ratios serving as a proxy for DO in the overlying water body (DO measured some decimeters away from the seafloor) (Schöne et al., 2021).

Due to its long lifespan and presence of annual growth patterns (Jones, 1980; Butler et al., 2013; Schöne, 2013) the ocean quahog, *A. islandica* can potentially serve as an accurately dated DO archive spanning several decades or centuries. The DO history may be assessed on even longer time-scales if Mn/Ca$_{shell}$ data of live-caught specimens from museum collections were used and/or crossdated specimens were studied. For the latter purpose, annual increment width series of specimens with overlapping lifespan are combined based on similar growth patterns to form longer chronologies that cover many generations of bivalves (Butler et al., 2013; Black et al., 2019). Its tolerance against severe oxygen depletion (Theede et al., 1969; Taylor, 1976; Oeschger, 1990; Oeschger and Storey, 1993; Strahl et al., 2011) makes the ocean quahog an ideal DO archive. However, its biogeographic distribution is not uniform in the Baltic Sea (Zettler et al., 2001; Darr et al., 2014). Therefore, it would be extremely useful if different bivalve species could be used interchangeably or alternatively to reconstruct the spatial and temporal development of DO.

Here, we have studied if *Astarte borealis* and *Astarte elliptica* record DO in a similar way as *A. islandica* and thus serve as alternative DO archives. According to existing laboratory experiments, *Astarte* spp. is slightly more tolerant against low DO than *A. islandica* (Theede, 1973; Dries and Theede, 1974) and more widely distributed in the Baltic Sea (Darr et al., 2014). Specimens of all three species were recently collected alive in the same region of the Fehmarn Belt, Baltic Sea. Data obtained herein on *A. islandica* (ontogenetic age range: 9 – 41 yrs; water depth: 21 m; DO range: 2.8 – 9.4 mL/L; temporal coverage: 1983 – 2020) supplemented such of a previous study of the same species from Mecklenburg Bight (7 – 19 yrs; 25 m; 1.8 – 8.9 mL/L; 1987 – 2001) (**Table 1**). Particular attention was paid to the relationship between DO and Mn/Ca$_{shell}$, ontogenetic Mn/Ca$_{shell}$ trends, lifespan, timing and rate of seasonal shell growth and clarity of growth patterns necessary to temporally align the chemical data measured in the shells. Results of this study will be of great relevance to reconstruct multiregional DO trends through time in the Baltic Sea. Given the broad biogeographic distribution of *A. elliptica* (Abbott and Morris, 1995) and *A. borealis* (Zettler, 2001) outside the Baltic Sea, similar studies on water oxygenation trends can likely be conducted at many other localities.

2 MATERIALS AND METHODS

Five specimens of *A. islandica* and three specimens of each, *A. elliptica* and *A. borealis*, were collected alive at Fehmarn Belt near the halocline on 29 June 2020 with van Veen grabs during cruise EMB239 with the R/V Elisabeth Mann Borgese (**Table 1**; **Figure 1**). *A. islandica* and *A. elliptica* co-occurred in 21 m (median grain size: 114 µm, organic content: 1.65 wt%), and *A.*

TABLE 1 | List of bivalves from the Baltic Sea used in the present study along with basic environmental data (monthly temperature, T, salinity, S, dissolved oxygen concentration, DO conc., and DO saturation, DO sat).

Specimen ID	Taxon	Ontogenetic age (yr)	#$\delta^{18}O$ samples	LA-ICP-MS:#spots, cal. yrs, ontog. yrs
Fehmarn Belt (FBR36): 54°18′59.50′′N, 011°33′00.00′′ E; 21m;				
1983-2020: T: -0.4–14.6°C; S: 10.9–26.5; DO conc.: 3.0–9.4 mL/L; DO sat.: 32.1–77.9%				
MLZ-FBR36-A4L	*Arctica islandica*	41		480, 1983–2020, 4–41
MLZ-FBR36-A5R	*Arctica islandica*	38	79 (43)	
MLZ-FBR36-A6L	*Arctica islandica*	9		207, 2015–2020, 4–9
MLZ-FBR36-A7L	*Arctica islandica*	10		202, 2012–2020, 3–10
MLZ-FBR36-A15L	*Arctica islandica*	10		393, 2012–2020, 3–10
MLZ-FBR36-A16L	*Arctica islandica*	21		441, 2005–2020, 6–21
MLZ-FBR36-A8L	*Astarte elliptica*	21	180 (70)	170, 2004–2020, 5–20
MLZ-FBR36-A9L	*Astarte elliptica*	27		134, 2003–2015, 10–21
MLZ-FBR36-A10L	*Astarte elliptica*	30		197, 1997–2015, 7–24
Fehmarn Belt (FBR06): 54°37'01.20"N, 011°00'36.00"E; 18m;				
1978-2019: T: -0.4–16.2°C; S: 10.9–26.8; DO conc.: 2.8–9.2 mL/L; DO sat.: 28.3–80.2%				
MLZ-FBR06-A1L	*Astarte borealis*	50		210, 1978–2019, 8–49
MLZ-FBR06-A2L	*Astarte borealis*	52		163, 1981–2019, 13–51
MLZ-FBR06-A3L	*Astarte borealis*	47	175 (31)	190, 1981–2018, 8–45
Mecklenburg Bight (St12): 54°18′59.50′′N, 011°33′00.00′′ E; 25 m;				
T: -0.5–16.9°C; S: 14.9–28.9; DO conc.: 2.0–8.9 mL/L; DO sat.: 24.5–77.1%				
MLZ-St12-A4R	*Arctica islandica*	19		329, 1987–2001, 5–19
MLZ-St12-A5R	*Arctica islandica*	15		326, 1991–2001, 5–15
MLZ-St12-A6R	*Arctica islandica*	14		373, 1991–2001, 4–14
MLZ-St12-A7L	*Arctica islandica*	7		183, 1997–2001, 3–7
MLZ-St12-A9R	*Arctica islandica*	8		151, 1998–2001, 5–8

All specimens were collected alive (Fehmarn Belt: 29 June 2020; Mecklenburg Bight: 25 October 2001). Last character of ID denotes left (L) or right (R) valve. Isotope samples in parentheses denote number of samples used to construct the seasonal age model. For details on the age model of specimens from Mecklenburg Bight, see Schöne et al. (2021).

borealis came from 18 m water depth (median grain size: 961 µm, organic content: 2.43 wt%) (**Figure 1** and **Table 1**). Immediately after collection, specimens were sacrificed in formalin and then preserved in 70 vol% ethanol. In the laboratory, soft parts were removed with a knife and empty shells washed with soap and water. Data obtained herein were combined with such of a previous study on live-collected *A. islandica* specimens from Mecklenburg Bight (**Figure 1**; for details see Schöne et al., 2021). Relevant data of the bivalves and the physical environmental parameters at both study regions are provided in **Table 1**.

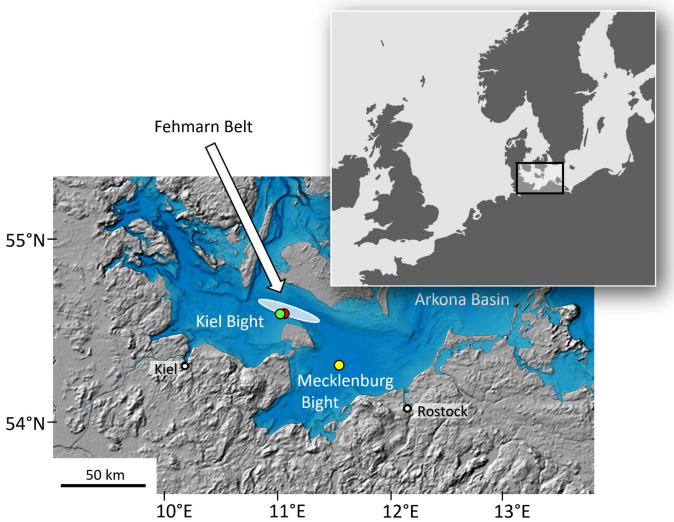

FIGURE 1 | Map showing sample localities in the Bay of Mecklenburg (yellow circle: St12, 54°18′59.50′′N, 011°33′00.00′′ E, 25 m water depth) and Fehmarn Belt (green circle: FBR36, 54°35'52.80"N, 010°51'28.80"E, 21 m; red circle: FBR06, 54°37'01.20"N, 011°00'36.00"E, 18 m). White oval denotes area where instrumental records came from. Map sources: inlet (upper right) modified after http://www.mygeo.info; bathymetry map modified after http://data.bshc.pro (Baltic Sea Bathymetry Database); last access: 27 Oct. 2021.

2.1 Sample Preparation

Samples were prepared according to standard sclerochronological techniques described recently in Schöne et al. (2021). Briefly, covered with a protective layer of metal epoxy resin, shells were cut along the axis of maximum growth with a low-speed saw at 175 to 225 rpm and a water-cooled 0.4 mm thick, diamond-coated saw blade (low diamond concentration blade, Buehler IsoMet 15LC). From that axis, two ca. 3 mm-thick slabs were cut, which were affixed (with metal epoxy) to glass slides with the cutting surfaces facing upward. These surfaces were then ground on F800 and F1200 grit SiC powder and highly polished with 1 μm Al_2O_3 suspension on a Buhler Microfloc cloth. After each step, samples were ultrasonically rinsed with tap water and then air-dried.

2.2 Growth Pattern Analysis

For shell growth pattern analysis, one polished section of each specimen was immersed in Mutvei's solution for 17 min under constant stirring at 37 to 40°C, then gently rinsed in deionized water and air-dried under the fume hood for ca. six hours (Schöne et al., 2005a). Mutvei-stained sections were viewed under a binocular microscope equipped with sectoral (= one-quarter) darkfield ring-light illumination (Schott VisiLED MC1000) and photographed with a Canon EOS 600D digital camera (**Figure 2A** upper panel + B). In addition, the other, unstained polished slab was studied under brightfield illumination (**Figure 2A** lower panel + C) as well as under a stereomicroscope (Zeiss Axio Imager.A1m) with circular polarized reflected light in conjunction with a differential interference contrast prism ("C-DIC method"; Danz and Gretscher, 2004) (**Supplements**). The C-DIC method was particularly useful to cross-verify annual growth patterns in *Astarte* spp.

Growth pattern analyses fulfilled two tasks. They were used to determine the ontogenetic ages of the studies specimens (**Table 1**) and to assign calendar years to annual increments (= portions between annual growth lines). Annual increment widths (**Supplements**) were measured to the nearest approx. 10 μm using the in-house software package Panopea (© Peinl and Schöne). These data were compared to weighted element-to-Ca averages (i.e., regression analyses were conducted) to reveal potential growth rate-related kinetic effects. In *A. elliptica* intra-annual growth patterns were visible after immersion in Mutvei's solution (**Figure 2B**). The changing widths of intra-annual growth increments agreed at large with changing seasonal growth rates inferred from the oxygen isotope alignment approach (see below). Mutvei-stained sections also facilitated the study of the geometry of internal shell growth patterns (e.g., **Figure 2B**) which is crucial to understand time-averaging of samples taken from the shells and to construct more precise seasonally resolved chemical chronologies.

2.3 Shell Oxygen Isotope Analysis

As described above, shell oxygen isotope data were used to temporally contextualize the growth record, determine the timing of growth line formation, and ascertain the changing rate of seasonal shell growth. Since *A. islandica* from the Baltic Sea tends to be very thin-shelled compared to conspecific specimens from well-oxygenated and fully marine sites (e.g., Arntz and Weber, 1970), and the growth patterns of *A. elliptica* exhibit strong undulations, sampling in these two species was completed on the outer shell surface of specimens MLZ-FBR36-A5 (*A. islandica*; N=79) and MLZ-FBR36-A8 (*A. elliptica*; N=72). In *A. borealis* (MLZ-FBR06-A3), aragonite powder samples (N=173) were micromilled from cross-sections (for a graphic representation of the sampling methods see Peharda et al., 2019). Prior to sampling, the periostracum (and adhering manganese oxides) and the outermost portion of the external shell surface were physically removed with grinding paper (P320 to P800) and/or a glass fiber brush. Aragonite powder samples were obtained by hand from the outer shell surface using a conical SiC drill bit operated in a milling device that was firmly attached to a binocular microscope. In case of surface milling, approx. 1 cm long sample swaths (approx. 100 μm wide and 20 μm deep) were taken at nearly equidistant intervals parallel to the growth patterns.

Each milling step yielded approx. 30 to 70 μg of aragonite powder. Samples were reacted with water-free phosphoric acid for two hours in He-flushed 12 mL borosilicate exetainers at 72°C. CO_2 gas in the headspace was measured in a Thermo Fisher MAT 253 continuous flow – isotope ratio mass spectrometer coupled to a GasBench II. Stable isotope ratios were calibrated against an NBS-19 calibrated Carrara Marble ($\delta^{18}O$ = −1.91 ‰) distributed by IVA Analysentechnik GmbH & Co. KG. Results are given in per mil (‰) relative to the Vienna Pee Dee Belemnite isotope scale. The 1σ long-term accuracy based on blindly measured NBS-19 samples (N = 421) is better than 0.04 ‰ for $\delta^{18}O$. Differences in acid fractionation factors of the reference material (calcite) and shells (aragonite) remained unconsidered, because the data were used in conjunction with the paleothermometry equation by Grossman and Ku (1986) which likewise did not consider these acid fractionation factors (for more detailed explanation see *Materials and Methods* section in Füllenbach et al., 2015: section *Relationship Between Mn/Ca$_{shell}$ Data and DO Concentration*).

2.4 *In-Situ* Chemical Analysis: LA-ICP-MS

The chemical composition of the shells was measured in the remaining polished slabs by means of laser ablation – inductively coupled plasma – mass spectrometry (LA-ICP-MS) in spot mode. In this paper, the focus was placed on manganese (Mn), and reference was given to barium (Ba) and magnesium (Mg) values. For some additional elements (Li, B, Na, K, Sr), the reader is referred to Supplements. Analyses were completed with a 193 nm ArF Excimer laser (ESI NWR193) coupled to an Agilent 7500ce quadrupole ICP-MS. Spots with a diameter of 55 μm and a midpoint spacing of 85 μm were placed along the ventral margins of the shells, within the inner portion of the outer shell layer. Laser repetition rate was 10 Hz. The laser energy on the samples attained approx. 3 J/cm^2. Each analysis consisted of 15 s of background, 30 s of ablation, and 20 s of washout time. Accuracy and precision of the data were assessed through comparison with reference materials USGS MACS-3 and BCR-

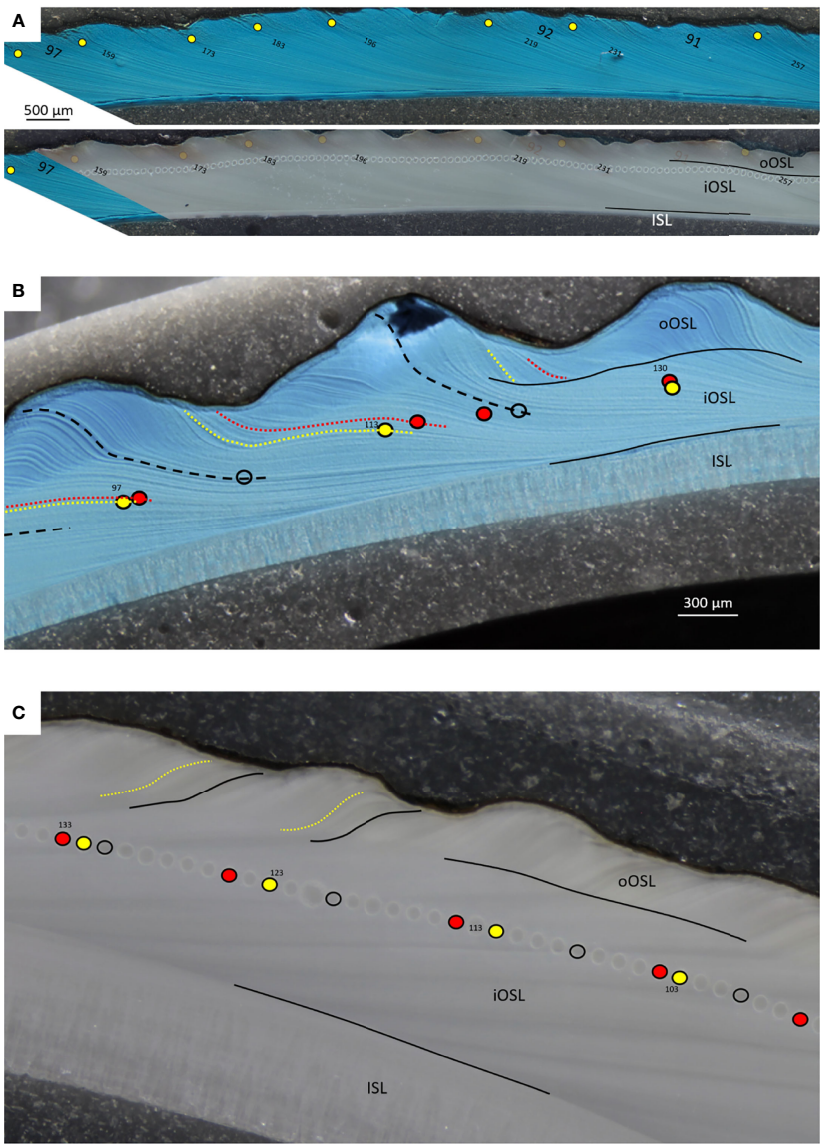

FIGURE 2 | Growth patterns in shells of *Arctica islandica* (**A**, specimen MLZ-FBR36-A4L), *Astarte elliptica* (**B**, MLZ-FBR36-A9L) and *Astarte borealis* (**C**, MLZ-FBR06-A1L). (**A,** upper panel + **B**) = sectoral darkfield illumination; (**A,** lower panel and **C**) = brightfield illumination (with partly numbered LA-ICP-MS spots). Yellow circles and yellow dotted lines indicate seasonal magnesium peaks, red circles (LA-ICP-MS spots) and lines stand for manganese peaks, and black open circles in *Astarte* spp. denote Mn minima. Bold numbers in **A** = calendar years (e.g., "97" = 1997). In *A. islandica*, only one annual growth line is developed which forms in late fall and is associated with the seasonal Mg peak. In Mutvei-stained sections (**A** upper panel), the annual growth lines were often difficult distinguish from disturbance lines. In such cases, comparison with polished cross-sections (**A** lower panel) was a great help, because distinct brown annual bands were occasionally developed with the Mg maxima occurring in their center. In *Astarte* spp., two annual growth lines can be distinguished which delimit a dark band (dark blue after immersion in Mutvei's solution, **B**, and grey in polished sections, **C**), i.e., a faint, Mg-rich line at the beginning and a distinct Mg-depleted line at the end. The dark band consisted of a series of very narrow intra-annual growth lines indicating slow winter growth. Intra-annual growth lines approached the outer shell surface at an increasingly steep angle toward the end of the growth band. With the beginning of the new growing season (lighter blue or grey in **B**, **C**, respectively), the angle became much shallower indicating fast shell growth. Faint black lines were used show the boundary between the different shell layers, i.e., the outer and inner portions of the outer shell layer (oOSL, iOSL) and inner shell layer (ISL). Note that the ISL in *A. islandica* is almost completely dissolved **(A)**, whereas both astartids show thick inner shell layers. In *A. elliptica*, the spiral rides of the outer shell sculpture (approx. one per year) are mirrored in the wavy boundary between the two sublayers of the OSL **(B)**, whereas the boundary between the oOSL and iOSL in *A. borealis* is much less wavy **(C)**.

2G as well as JCt-1 as quality control materials (QCMs) (**Supplements**). NIST SRM 610 and 612 were used as calibration materials. Preferred values for calibration and reference materials were taken from the GeoReM database (http://georem.mpch-mainz.gwdg.de/, application version 30; last access: 15 May 2021; Jochum et al., 2005; Jochum et al., 2011). ^{43}Ca was used as the internal standard. The time-resolved signals were processed using LAtools (Branson et al., 2019). To

compute molar element-to-Ca ratios, a Ca concentration of 380,000 µg/g was assumed following Marali et al. (2017a).

To compare the shell element chemical data of different specimens or species with each other, or compare the shell element chemistry with environmental data, a set of mathematical transformations is required, which are described in the following two sections. Firstly, it needs to be ensured that each data point represents the same amount of time and that a calendar axis is added to the data (section *Seasonal Shell Growth Models and Mathematical Resampling*). Secondly, trends related to ontogenetic age or growth rate as well as vital effects controlling the incorporation of elements into the shell need to be mathematically eliminated as effectively as possible (section *Detrending of Mn/Ca$_{shell}$ Data*).

2.5 Seasonal Shell Growth Models and Mathematical Resampling

The timing and rate of shell growth typically varies through ontogeny as well as between specimens, species and localities. Equally sized samples taken from the shells thus represent different amounts of time. Likewise, the time interval between consecutive samples differs, even if sampling was completed at the same spacing. To enable a direct comparison of the chemical data, mathematical resampling is crucially required (Schöne, 2008; Hallmann et al., 2011). It will adjust the data to a common temporal resolution. The first step is to properly align the growth record based on the species-specific seasonal age model. Once the precise date of the center of each sample (e.g., LA spot) is known, missing data between samples can be obtained by linear interpolation. The resulting curve is then resampled to obtain an uninterrupted artificial time-series with daily resolution, which can be used, for instance, to compute monthly or annual averages.

Here, the species-specific and locality-specific timing and rate of seasonal shell growth was determined with the stable oxygen isotope method described by Schöne et al. (2007). For this purpose, measured $\delta^{18}O_{shell}$ values were arranged in consecutive order until the best fit was achieved with the shape of the predicted shell oxygen isotope curve (pseudo-$\delta^{18}O_{shell}$ curve). The latter was computed from instrumental temperature, T, and $\delta^{18}O_{water}$ values using the paleothermometry equation by Grossman and Ku (1986; with a PDB-SMOW scale correction of –0.27 ‰ following Gonfiantini et al., 1995) solved for predicted $\delta^{18}O_{shell}$:

$$Predicted\ \delta^{18}O_{shell} = \frac{20.60 + 4.34 \times \left(\delta^{18}O_{water} - 0.27\right) - T}{4.34} \quad (1)$$

In the absence of direct measurements of $\delta^{18}O_{water}$, respective values were estimated from instrumental salinity data, S, using the local freshwater mixing line (Schöne et al., 2005b):

$$\delta^{18}O_{water} = 0.30 \times S - 10.36 \quad (2)$$

Based on the known distances and time intervals between the isotope samples, daily growth curves were computed. For comparison with each other, the growth curves were normalized. Then, the seasonal growth curves of several years for which at least eight samples were available (*A. islandica* MLZ-FBR36-A5: 4 seasonal growth curves; *A. elliptica* MLZ-FBSCR36-A8: 7 curves; *A. borealis* MLZ-FBR06-A3: 4 curves; full data set given in **Supplements**) were arithmetically averaged to obtain species-specific seasonal growth models (**Figure 3**). Cumulative (normalized) growth curves formed the basis to add a time axis to the LA-ICP-MS data. Based on the relative position of a LA-ICP-MS spot within the annual growth increment (center of the annual growth line = zero), the cumulative growth curve provided the corresponding calendar date.

2.6 Detrending of Mn/Ca$_{shell}$ Data

For calibration and comparison with environmental data, ontogenetic age-related trends (**Figure 5**) were mathematically removed from each Mn/Ca$_{shell}$ series. For this purpose, the monthly Mn/Ca$_{shell}$ data of each specimen were first plotted against ontogenetic age and the decline through life estimated with exponential functions. Following our previous study (Schöne et al., 2021), instead of producing dimensionless Mn/Ca$_{shell}$ data, the Mn/Ca$_{shell}$ level at the intercept (age zero) was set as an anchor point, and the monthly Mn/Ca$_{shell}$ values of later stages of life increased by the difference (offset) between this anchor point and the predicted Mn/Ca$_{shell}$ value at the respective stage of life. Note, that we also tested a species-specific detrending approach as in Schöne et al. (2021), by which the average ontogenetic Mn/Ca$_{shell}$ trend computed from all conspecific specimens was used to detrend the individual chronologies, but the resulting Mn/Ca$_{shell}$ data were linked less strongly to DO than by employing the age trend of each individual specimen.

To account for growth rate-related effects, annual (= growing season averages) Mn/Ca$_{shell}$ data were plotted against annual increment widths. From such cross plots, species-specific linear regression models were computed. As in the detrending technique described earlier, an anchor point was selected (for each species), here, the broadest increment, and the difference between this anchor point and the predicted Mn/Ca$_{shell}$ value for the respective annual increment added to its monthly Mn/Ca$_{shell}$ values. Note that through this treatment, the Mn/Ca$_{shell}$ of slower growing shell portions were artificially lifted to higher levels as if no Mn/Ca$_{shell}$ decline had occurred in later, slower growing stages of life. In case of *A. islandica*, new data from Fehmarn Belt were combined with such from our previous study at Mecklenburg Bight (Schöne et al., 2021). We refrained from adjusting the monthly data to monthly growth rate differences, because intra-annual increment curves were not available and the seasonal growth models were not deemed precise enough for this purpose.

To consider both Mg/Ca$_{shell}$ and growth rate-related effects on shell manganese content, raw Mn/Ca$_{shell}$ data were first plotted against Mg/Ca$_{shell}$ values. The relationship between the two elements was estimated with species-specific exponential equations. The Mn/Ca$_{shell}$ value at the lowest Mg/Ca$_{shell}$ value (of each species) was chosen as the anchor point and the offset from the anchor point to the predicted value added to the Mn/Ca$_{shell}$

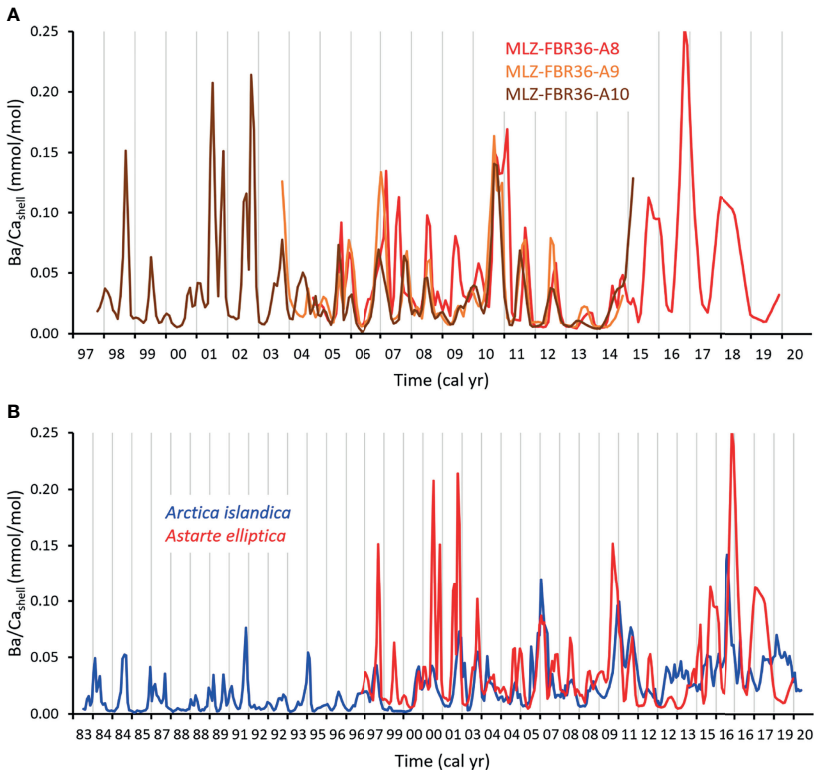

FIGURE 3 | Monthly Ba/Ca$_{shell}$ chronologies validate the proper temporal alignment of the shell data. Chronologies show a strong running similarity between specimens of the same species (example from *A. elliptica*) **(A)** as well as across species boundaries **(B)**. Chronologies in **(B)** represent the average of five specimens of *A. islandica* and three specimens of *A. elliptica*, respectively.

value. Subsequently, the data were corrected for growth rate-related trends following the description above.

As in our previous study at the Bay of Mecklenburg (Schöne et al., 2021), only the seasonal Mn/Ca$_{shell}$ extremes (this time: species averages) were compared to respective seasonal DO minima and maxima. This approach predominantly accounts for the incompleteness of instrumental data, in particular DO. Research cruises (during which respective measurements were completed) were often conducted during times of the occurrence of seasonal hypoxia or close to the time of the year where highest oxygenation occurred. Therefore, the seasonal DO extremes were most reliably recorded. The complete dataset (monthly pairs of Mn/Ca$_{shell}$ vs. DO) is provided in the **Supplements**.

2.7 Instrumental Data

Instrumental data (temperature, salinity, DO concentration) were obtained from the Leibniz Institute for Baltic Sea Research Warnemünde, IOW, from their website at https://odin2.io-warnemuende.de/as well as the Baltic Nest Institute from their website at http://nest.su.se/(last access: 25 March 2021) for stations and water depths in the vicinity of the shell collection sites (**Figure 1**). It needs to be pointed out that the instrumental measurements were not conducted at the seafloor where the bivalves dwelled and inhaled water, but some decimeters away from the seafloor. Here, the Mn/Ca and DO values of the water likely differed from such directly at the sediment-water interface where the bivalves lived, but co-varied with such. This piece of information needs to be kept in mind during data interpretation. Since the environmental data were temporally incomplete, linear interpolation was applied to fill gaps. The resulting curves were then resampled at daily resolution. From these values, monthly and annual averages were computed for comparison with the chemical data of the shells. To construct the seasonal shell growth model, long-term daily averages were computed. Due to insufficient instrumental temperature and salinity data required to compute DO saturation data from DO concentration values (Benson and Krause, 1984), the latter were reported instead. As demonstrated in Schöne et al. (2021), DO concentration and DO saturation curves are largely similar in this region of the Baltic Sea justifying the comparison of Mn/Ca$_{shell}$ with DO concentration.

3 RESULTS

3.1 Lifespan and Annual Shell Growth

In all three studied species, annual growth lines were discernable with sectoral darkfield illumination after immersion in Mutvei's solution (**Figure 2**). The old-grown *A. islandica* specimen MLZ-

FBR-A4 also showed distinct brown annual bands and lines in the polished ventral margin when viewed with brightfield illumination (**Figure 2A**, lower panel). Specifically in younger ocean quahogs, the annual growth patterns were often more clearly developed in the hinge portions (condensed growth record) than the ventral margin, and used to validate the ventral margin growth record. The occurrence of disturbance lines (reflecting non-periodic interruptions or slow-down of shell growth) in the ocean quahogs made the recognition of annual growth lines a challenging task. As long as the cutting axis was exactly perpendicular to the growth lines, the C-DIC method provided an alternative means to detect annual growth lines in polished sections (**Supplements**). The annual nature of the growth patterns was confirmed by periodic Mg/Ca_{shell} and $\delta^{18}O_{shell}$ oscillations which were also reported from numerous other bivalve species (Jones and Quitmyer, 1996; Kubota et al., 2017; Hausmann et al., 2019) including *A. islandica* (Schöne, 2013; Shirai et al., 2014). The presence and proper recognition of annual growth patterns was further evidenced by coherent Ba/Ca_{shell} chronologies, both among conspecific specimens and across species boundaries (**Figure 3**). Ba/Ca_{shell} typically agrees well among specimens from the same site (Gillikin et al., 2006) and thus serves as a crossdating tool (Marali et al., 2017b), although the environmental drivers of Ba/Ca_{shell} change in *A. islandica* remain largely unknown.

In contrast to *A. islandica*, which formed just one annual growth line per year (**Figure 2A**), after immersion in Mutvei's solution, both *Astarte* species showed two growth lines per year delimiting a dark blue-stained growth band (**Figures 2B, C**). The first, faint line occurred at the beginning of this growth band and was associated with the seasonal Mg/Ca_{shell} maximum, whereas a second, stronger growth line was observed at the end of the dark blue band and associated with the seasonal Mg/Ca_{shell} minimum. According to annual growth pattern analysis, the ontogenetic ages ranged between 9 and 52 years (**Table 1**; respective annual counts were done in the ventral margins supported by data of the hinges). *A. borealis* attained the longest lifespan, followed by *A. islandica* (maximum of 41 years) and *A. elliptica* (27 years).

Compared to their sizes, the shells of *A. islandica* were notably thin. For example, specimen MLZ-FBR36-A4 measured 6 cm in height, but the shell was barely 1 mm thick (measured half way between the hinge and the ventral margin; **Figure 2A**). As shown in **Figure 2A**, the inner shell layer was extremely thin and showed signs of erosion. Relative to their overall size, both *Astarte* species, however, had thicker shells (MLZ-FBR36-A9L: 2.1 cm height; 1.2 mm thickness measured half way between the hinge and ventral margin; **Figures 2B, C**).

3.2 Timing and Rate of Seasonal Shell Growth

As revealed by the stable oxygen isotope alignment technique, the timing and rate of seasonal shell growth at Fehmarn Belt differed slightly among the three studied species (**Figure 4**). *A. islandica* mainly grew shell between December and August of the following year. Growth was retarded during the remainder of the growing season. The annual growth line (Mg-rich) formed between mid-October and mid-November (**Figures 2A**, **4A**), i.e., ca. two months after the seasonal temperature maximum, which is largely in agreement with previous observations (Schöne, 2013). For comparison, the seasonal growth model from Mecklenburg Bight is also depicted in **Figure 4A** (pale blue) demonstrating that the growth line formation occurred several weeks earlier than at Fehmarn Belt. In *A. elliptica* and *A. borealis*, a Mg-rich growth line (compare **Figures 2B, C**) formed nearly contemporaneously with that in the ocean quahog, i.e., between mid-October and end of November (**Figures 4B, C**). A second growth line (compare **Figures 2B, C**) was associated with the seasonal Mg minimum and laid down in January/February, i.e., near the end of a slow growth period (**Figures 4B, C**). The latter was visually expressed as a dark grey (or dark blue-stained) growth band (compare **Figures 2B, C**). Previous studies likewise concluded the dark growth band in these two astartids formed during the cold season (Trutschler and Samtleben, 1988; Moss et al., 2021). The cumulative growth curves of the studied species were not particularly sinusoidally shaped (**Figure 4**), reflecting that shell growth rates did not vary a lot throughout the year. Accordingly, weighted monthly (annual) averages of trace element data do not deviate significantly from arithmetic averages.

A. elliptica was the only species that revealed intra-annual growth patterns clearly enough to be studied (**Figure 2B**). The $\delta^{18}O_{shell}$-based reconstruction of the seasonal growth curve (**Figure 4B**) of this species compared well to the changing width of the intra-annual growth increments (**Figure 2B**). Narrowest intra-annual increments occurred between the Mg-rich and the Mg-poor growth lines, i.e., within the dark blue-stained growth band. The growth lines in this shell portion approached the outer shell surface at a very steep angle. Thereafter, the shells were stained lighter blue by Mutvei's solution (= less organics, relatively more $CaCO_3$), the intra-annual increments broadened and the angle between intra-annual growth lines and the shell surface decreased reflecting faster shell growth (compare **Figure 2B**). Since the time represented by intra-annual growth increments remains unresolved and the intra-annual growth lines could not always be unequivocally identified, the intra-annual increment widths were not measured. Noteworthy, the striking sculpture of the outer shell surface of *A. elliptica* (compare **Figure 2B**) provided an approximate estimate of the ontogenetic age of the specimens. In many instances, one spiral ridge formed per year (but see Trutschler and Samtleben, 1988).

3.3 Mn/Ca_{shell} Chronologies

In all three studied species, Mn/Ca_{shell} values showed a non-linear decrease during ontogeny (**Figure 5**). In *A. islandica* this decrease was associated with a distinct decline in seasonal variability (**Figure 5A**). For example, this species attained monthly averages of up to approx. 220 µmol/mol and seasonal ranges of nearly 200 µmol/mol between age three and six (months 36 and 72) and lowest values of 1 µmol/mol and seasonal ranges of less than 5 µmol/mol at age 36 (month 432) (**Figure 5A**). In *A. elliptica*, monthly maxima and seasonal swings during youth (age six to nine, month 72 to 108)

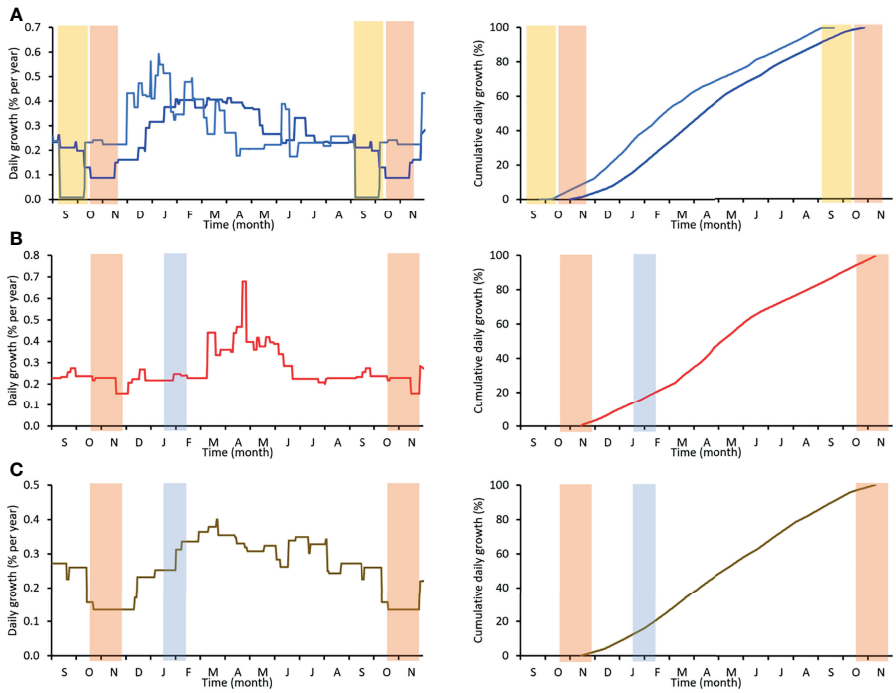

FIGURE 4 | Seasonal growth models of the three studied species based on the oxygen isotope alignment technique. Left panel: daily growth rates, right panel: cumulative growth curves. **(A)** *A. islandica*, station FBR36 (Fehmarn Belt) is brilliant blue, St12 (Mecklenburg Bight) in pale blue; **(B)** *A. elliptica*, FBR36; **(C)** *A. borealis*, FBR06 (Fehmarn Belt). Vertical bars represent annual growth lines. Red, yellow = Mg-rich line at Fehmarn Belt and Mecklenburg Bight, respectively; blue = Mg-depleted growth line. In *Astarte* spp., the red and blue lines delimit a grey (or Mutvei blue-stained) growth band. Data from Mecklenburg Bight taken from Schöne et al. (2021).

remained well below that of the ocean quahog and equaled 120 µmol/mol and up to approx. 80 µmol/mol, respectively, and all-time minima of 5 µmol/mol were reached at age 23 (month 276) (**Figure 5A**). Similar values were measured in coeval *A. islandica* specimens. *A. borealis* reached highest Mn/Ca$_{shell}$ values of 114 µmol/mol at the age of eight (month 96), ca. 40 µmol/mol at age 23 (month 276), and a minimum of 6 µmol/mol at age 35 (month 420). Highest seasonal amplitudes during youth barely exceeded 45 µmol/mol (**Figure 5A**). In contrast to Mn/Ca$_{shell}$ values, Mg/Ca$_{shell}$ values increased non-linearly through lifetime (**Figure 6**). For greater clarity, only one of the longest chronologies of each species is depicted in **Figure 6**. Note strong seasonal oscillations (in sufficiently resolved years) as in Mn/Ca$_{shell}$ chronologies.

When this ontogenetic age-related trend was mathematically removed (and the data plotted against calendar year), the detrended Mn/Ca$_{shell}$ curves not only revealed significant differences in level and seasonal variance between conspecific specimens as well as between species, but also some degree of running similarity (**Figure 7**). For example, in the 2010s, *A. islandica* specimen A4 barely exceeded 29 µmol/mol, whereas specimen A16 fluctuated between 43 and 131 µmol/mol (**Figure 7A**). The three remaining specimens from Fehmarn Belt were in closer agreement with each other and ranged between 37 and 280 µmol/mol (**Figure 7A**). Similar discrepancies in level were observed in the two *Astarte* species (**Figures 7B, C**). *A. elliptica* specimens A9 and A10 were in close agreement, specifically during 2004 and 2011, while specimen A8 showed, on average, approx. 20 µmol/mol higher values than the other two individuals and more than two to three times larger seasonal amplitudes (**Figure 7B**). In some years (mid 1990s), monthly Mn/Ca$_{shell}$ values of different *A. borealis* specimens deviated by nearly 750% (40 µmol/mol), while specimens MLZ-FBR06-A1 and A3 were much closer together (**Figure 7C**).

Aside from ontogenetic age, Mn/Ca$_{shell}$ data were also statistically significantly ($p < 0.0001$) linearly correlated to annual growth rate (**Figures 8A–C**) as well as other trace impurities (**Supplements**) which are governed by vital effects in *A. islandica* and numerous other species (e.g., Lorens and Bender, 1980; Palacios et al., 1994; Wanamaker et al., 2008; Wanamaker and Gillikin, 2019). The covariation between trace impurities suggests similar physiological effects have controlled the incorporation of these elements into the shell carbonate. In a first step, we targeted the correlation with growth rate. The strongest relationship between growth rate and Mn/Ca$_{shell}$ was found in *A. borealis* ($r = 0.83$; $p < 0.0001$, also for all subsequently given r-values of linear regression analyses unless otherwise stated) and some weaker covariation in *A. islandica* ($r = 0.60$) and *A. elliptica* ($r = 0.58$). Once these growth rate-related kinetic effects were mathematically eliminated, the Mn/Ca$_{shell}$ chronologies were in much closer agreement (**Figure 9**).

Mg/Ca$_{shell}$ molar ratios were chosen for the second detrending step, because they showed the strongest correlation

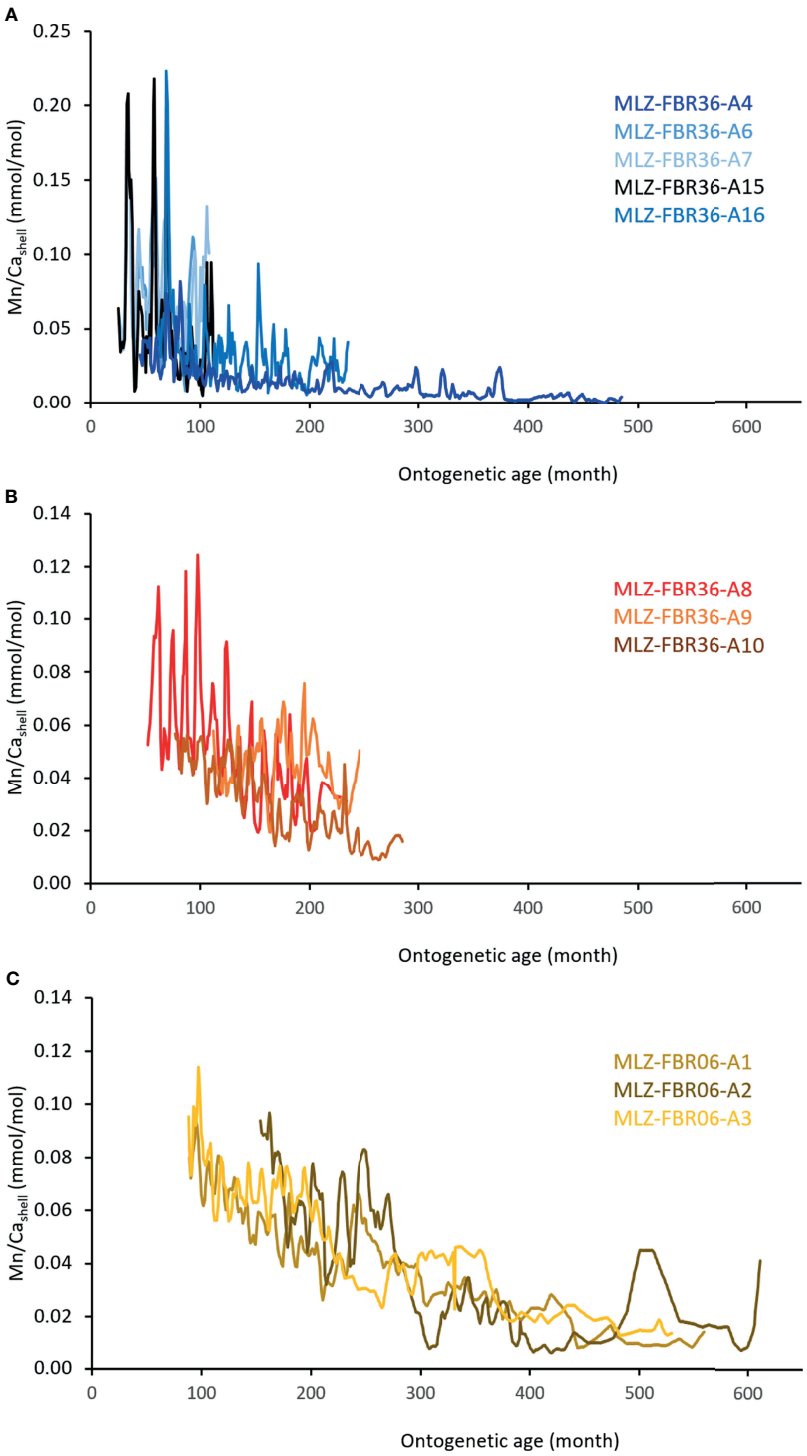

FIGURE 5 | Mn/Ca$_{shell}$ chronologies (monthly resolution) reveal striking ontogenetic trends to lower values. **(A)** *A. islandica*; **(B)** *A. elliptica*; **(C)** *A. borealis*.

with growth rate-detrended Mn/Ca$_{shell}$ among all measured element-to-Ca ratios (**Figures 8D–F**). This approach followed previous successful attempts to remove vital effects from a desired element-to-Ca ratio by normalization with another biologically controlled element-to-Ca value. Examples include Mn/Ca vs. Mg/Ca in fish otoliths (Limburg et al., 2011) as well as Li/Ca vs. Sr/Ca or Mg/Ca in foraminifera, cold-water corals and bivalves (Bryan and Marchitto, 2008; Case et al., 2010; Füllenbach et al., 2015; Rollion-Bard and Blamart, 2015). The double detrending approach (annual growth rate and Mg/Ca$_{shell}$)

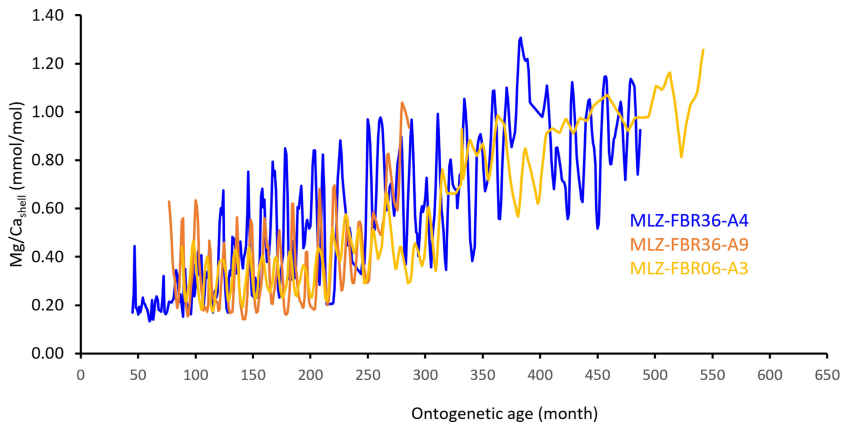

FIGURE 6 | Mg/Ca$_{shell}$ chronologies (monthly resolution) of long-lived specimens of *A. islandica* (MLZ-FBR36-A4), *A. elliptica* (MLZ-FBR36-A9) and *A. borealis* (MLZ-FBR06-A3) reveal distinct seasonal oscillations and a gradual increase through lifetime.

further constrained the similarity between the Mn/Ca$_{shell}$ curves and shifted them slightly closer together; **Supplements**) and more importantly, increased the agreement between Mn/Ca$_{shell}$ and DO, as outlined in the following.

3.4 Relationship Between Mn/Ca$_{shell}$ Data and DO Concentration

To evaluate the effect of the different detrending methods, Mn/Ca$_{shell}$ data of bivalves dwelling at the seafloor were compared with DO concentration measured some decimeters above seafloor (**Figure 10**). Ontogenetic age-detrended Mn/Ca$_{shell}$ data revealed only moderate linear correlations with seasonal DO extremes (R^2_{adj} range between 0.20 and 0.33), and the relationships varied notably between species, i.e., both the slopes and intercept deviated notably from each other (**Figure 10A**). Annual growth rate-detrending brought the species-specific regression lines much closer together, specifically that of *A. islandica* and *A. elliptica*, and also resulted in more coherent relationships between Mn/Ca$_{shell}$ and DO concentration (R^2_{adj} range between 0.31 and 0.53) (**Figure 10B**). The double-detrending approach further substantiated the correlations ($R^2_{adj}$of *A. islandica* = 0.38, *A. elliptica* = 0.56, and *A. borealis* = 0.43) (**Figure 10C**).

Despite double-detrending, however, the cross-plot of DO vs. Mn/Ca$_{shell}$ of *A. islandica* still exhibited a relatively large scatter which accounted for the relatively low R^2 values (**Figure 10C**). This largely resulted from a strong non-linear (here: exponential) relationship of Mn/Ca$_{shell}$ with DO in the younger shell portions of specimens MLZ-FBR36-A6, A7, A15 and A16 (**Figure 11A**). However, data of specimen MLZ-FBR-A4 plotted near the data of all specimens from Mecklenburg Bight (St12), i.e., individual differences rather than locality-specific differences prevailed (**Figure 11A**). A linear regression was performed on the DO concentrations and the logarithm-transformed Mn/Ca$_{shell}$ data to explore their potential significant relationship provided by p-values (see **Supplements**). For all except two specimens (FBR36-A16 and St12-A7), p was better than 0.05. In contrast, after the age of ten, Mn/Ca$_{shell}$ data of all *A. islandica* were strongly linearly correlated to DO (R^2_{adj} = 0.56; p < 0.0001) (**Figure 11B**). More importantly, the regression lines of the three species showed more similar slopes if data from the first nine years of life of the ocean quahog were omitted (*A. islandica*: −39 instead of −71, *A. elliptica*: −57, and *A. borealis*: −40 µmol/mol Mn/Ca$_{shell}$ per mL/L DO) (**Figure 11B**). When the data of all three species were combined in a single linear regression model, the adjusted R^2 value equaled 0.27, whereas a combination of *A. islandica* and *A. elliptica* provided a much higher adjusted R^2 value of 0.53. The *p*-values of all linear regression analyses were smaller than 0.0001 unless otherwise stated (**Supplements**).

Tentative predictive models for the three studied species are depicted in **Figure 12**. As above, for *A. islandica* only data from age ten onward were considered. According to these models, Mn/Ca$_{shell}$ data of *A. elliptica* can provide the most precise DO estimates, i.e., ± 1.5 mL/L. Slightly larger 1σ uncertainties are involved when *A. islandica* or *A. borealis* are used (both: ± 1.6 mL/L DO). A combination of data from *A. elliptica* and *A. islandica* is associated with an uncertainty of ±1.5 mL/L DO, and a mix of all studied specimens comes with an uncertainty of ±1.7 mL/L DO (**Supplements**). Following these transfer functions, in *A. islandica*, *A. elliptica* and *A. borealis*, an increase by 10 µmol/mol Mn/Ca$_{shell}$ reflects a decrease in DO by 1.44, 0.98, and 1.08 mL/L, respectively.

4 DISCUSSION

The present study adds further support to the hypothesis that molar Mn/Ca data of bivalve shells can provide temporally well-constrained records of DO in the free water column (Zhao et al., 2017a; Schöne et al., 2021). Like other redox-sensitive elements, manganese becomes dissolved (as Mn^{2+}) under reducing conditions (Hem, 1963; Balzer, 1982; Rue et al., 1997) and – against thermodynamic expectations – can remain for a while in this bioavailable form even under the presence of oxygen (Tebo,

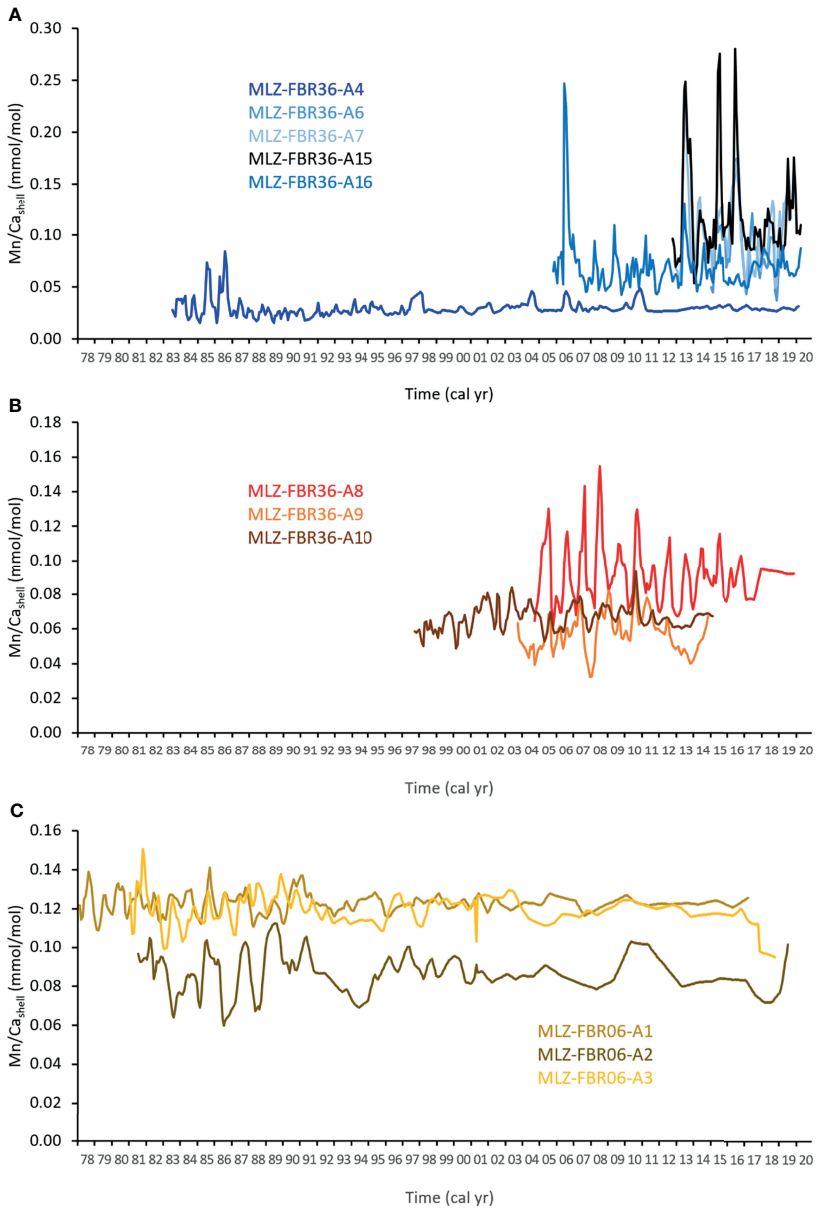

FIGURE 7 | After removal of ontogenetic age-related trends (compare **Figure 5**), Mn/Ca$_{shell}$ chronologies (monthly resolution) reveal distinct differences between conspecific specimens during the same calendar year. **(A)** *A. islandica*; **(B)** *A. elliptica*; **(C)** *A. borealis*.

1991), possibly mediated by organic substances (Kremling and Petersen, 1978). Relative to permanently well-oxygenated settings in the North Atlantic, manganese was significantly enriched in studied bivalve shells from the Baltic Sea (this study and Schöne et al., 2021). For example, shells of *A. islandica* from nearshore coastal sites in NE Iceland contained, on average, only 2 µmol/mol Mn/Ca$_{shell}$ and extremes barely reached 5 µmol/mol (Marali et al., 2017a). In contrast, respective values in conspecific specimens from the Fehmarn Belt and Mecklenburg Bight were, on average, 21 times higher (approx. 42 µmol/mol), and peaks (undetrended monthly data) can attain more than 300 µmol/mol Mn/Ca$_{shell}$ (Schöne et al., 2021).

As shown here, besides *A. islandica* two other species, i.e., *A. elliptica* and *A. borealis* can likewise serve as proxy archives for dissolved oxygen levels in the water column. Once corrected for shell growth rate-related kinetic effects and (some) vital effects, Mn/Ca$_{shell}$ data (age ten onward in *A. islandica*) of bivalves living at the seafloor are statistically significantly ($p < 0.0001$) correlated to DO concentration measured some decimeters above the sediment surface (r = –0.66 to –0.75, corresponding to 43 to 56% explained variability) (**Figure 12**). According to the tentative models developed here, *A. elliptica* can provide slightly more precise DO data (± 1.5 mL/L) than *A. islandica* or *A. borealis* (± 1.6 mL/L).

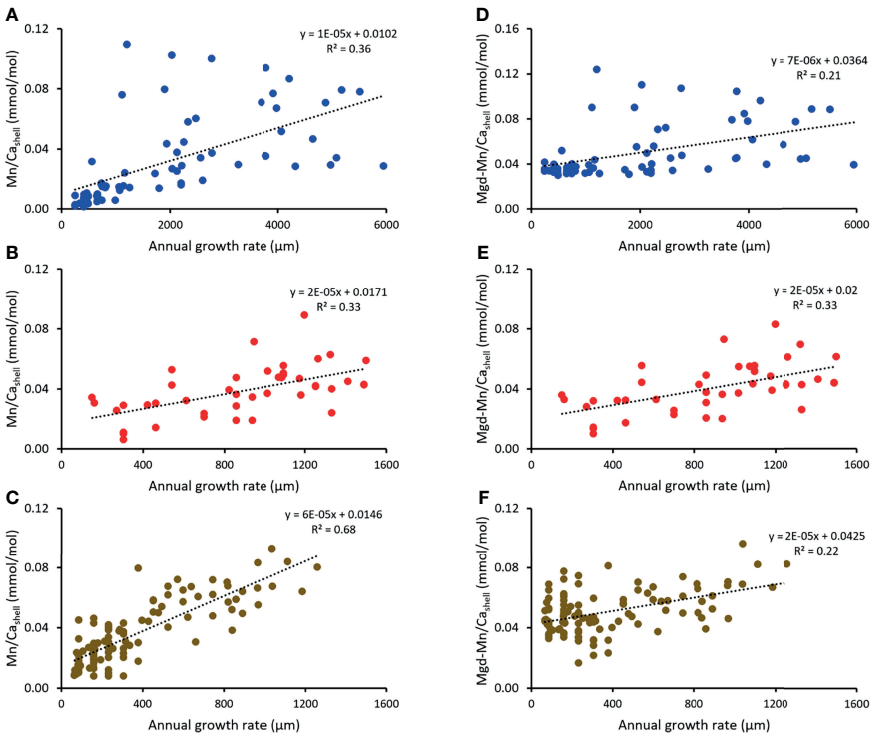

FIGURE 8 | Linear relationship between monthly Mn/Ca$_{shell}$ and annual growth rate before **(A-C)** and after detrending with Mg/Ca$_{shell}$ data **(D-F)**. **(A, D)** *A. islandica*, station FBR36; **(B, E)** *A. elliptica*, FBR36; **(C, F)** *A. borealis*, FBR06. All correlations were highly significant at $p < 0.0001$.

4.1 Advantages and Disadvantages of the Three Studied Species for DO Reconstructions

The prediction interval (**Figure 12**) certainly is a relevant criterion to determine which species might be the most suitable archive to reconstruct DO, but no major differences were observed between the three species (uncertainties of ±1.5 to 1.6 mL/L DO). Several other aspects should be considered as well including longevity, continued shell production under low DO levels and fluctuating salinity, distinctness of annual growth lines, growth pattern geometry and temporal resolution.

Shells of the ocean quahog in the Baltic Sea were considerably thinner than at most other sites. For example, the oldest specimen hardly measured more than one millimeter in thickness (**Figure 2A**). Predominantly, this resulted from a very thin, severely eroded or even missing inner shell layer (**Figure 2A**; see also Schöne, 2013). Like the two *Astarte* species, to survive under hostile environmental conditions, the ocean quahog switches into an anaerobic metabolism during which acidic metabolites are generated which are subsequently neutralized by the dissolution of inner shell surfaces (Crenshaw, 1980; Oeschger, 1990; Oeschger and Storey, 1993). However, *A. islandica* can also undergo self-induced anaerobiosis without a clear external trigger (Taylor, 1976; Oeschger, 1990). Perhaps, the ocean quahog thus spent more time in anaerobiosis than the other two species, and consequently, its shell experienced stronger dissolution of inner shell surfaces. With thinner, more fragile shells, the bivalve is less well protected against predators and possibly prone to damage by bottom-trawling (Rumohr and Krost, 1991) and may thus not attain the extraordinary lifespan reported from well-oxygenated sites in the North Atlantic, i.e., up to 500 years (Schöne, 2013; Butler et al., 2013). At least, the ontogenetic age of the oldest and largest specimen (**Table 1**), arbitrarily selected for the present study, remained well beyond the longevity for which *A. islandica* is renowned. Studied *A. borealis* attained higher ages than *A. islandica* (**Table 1**).

While all three studied species can survive hypoxic, anoxic and even euxinic conditions for several months (Theede et al., 1969; Weigelt & Rumohr, 1986; Oeschger, 1990; Oeschger and Storey, 1993) and resist large salinity swings (von Oertzen and Schlungbaum, 1972; von Oertzen, 1973), biomineralization rates of *A. islandica* were more severely affected by adverse environmental conditions than such of *Astarte* spp. Annual growth patterns of *A. islandica* were much more difficult to identify than typically at well-oxygenated, fully marine sites and less distinct than in the two Astartidae. In the ventral margin, the annual growth lines were only faintly developed and could hardly be distinguished from disturbance lines (**Figure 2A**). It thus took considerable efforts to temporally contextualize the shell portions of the ocean quahog in this region. Besides disturbance lines, several other findings suggested *A. islandica* experienced physiological stress as outlined in the following. With a maximum shell size increase of 6 mm per year it grew four to five times faster than *Astarte* spp., but annual growth rates

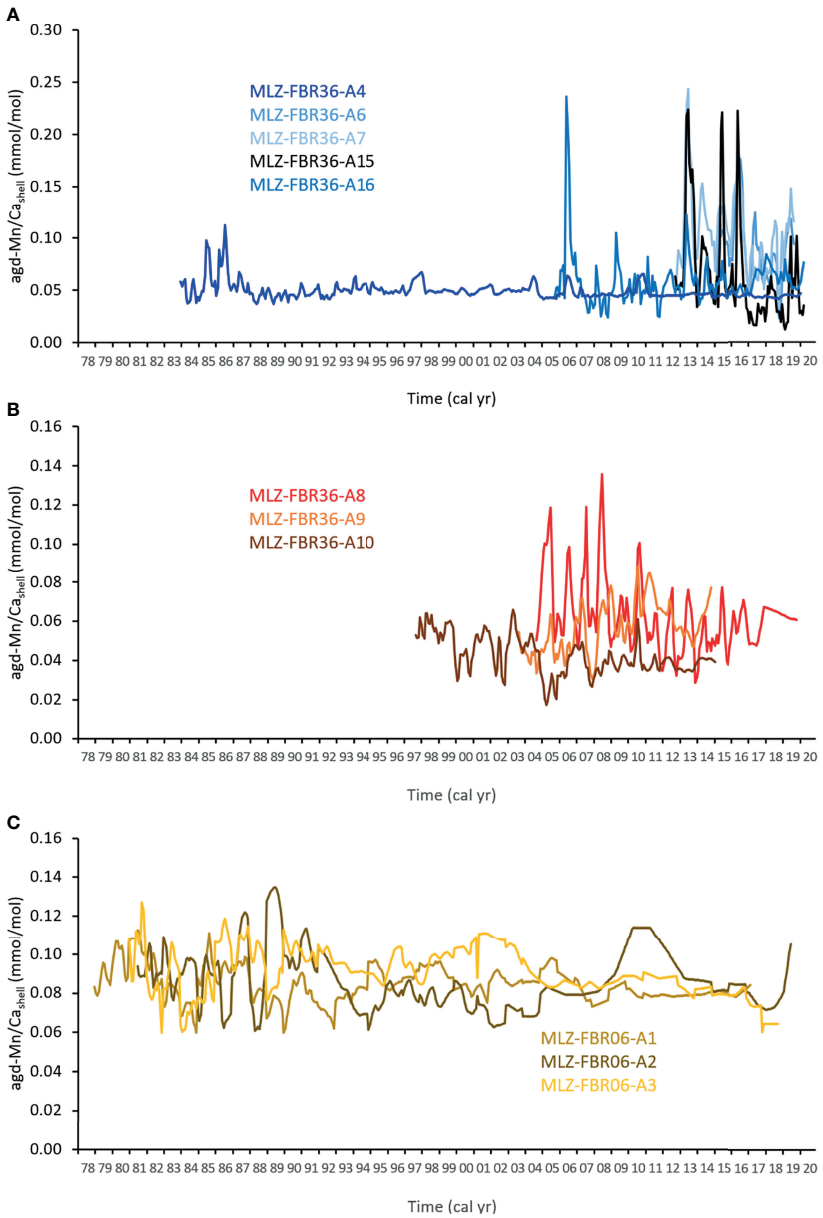

FIGURE 9 | After removal of annual growth rate-related trends (compare **Figures 8A–C**), Mn/Ca$_{shell}$ chronologies (monthly resolution; agd, annual growth rate detrended) plotted closer together and revealed a larger degree of running similarity. **(A)** *A. islandica*; **(B)** *A. elliptica*; **(C)** *A. borealis*.

remained approx. two to four times below that observed in this species at well-oxygenated, stenohaline sites in the North Atlantic (e.g., up to 20 mm per year around the coasts of the British Isles; personal observation, BRS). While food supply was certainly not a limiting growth factor, because the Baltic Sea is heavily eutrophicated (Conley et al., 2007), variable salinity and low-oxygen stress (**Table 1**) could have adversely affected shell production rates. The ocean quahog survives salinity stress better than *Astarte* (von Oertzen and Schlungbaum, 1972; von Oertzen, 1973), but likely on the expense of a reduced biomineralization rate. If more energy needs to be devoted to osmoregulation, less energy is available for growth and reproduction. Furthermore, the physiological resistance of *A. islandica* against oxygen deficiency and hydrogen sulfide is significantly lower than that of the *Astarte* spp. (von Oertzen and Schlungbaum, 1972; von Oertzen, 1973; Theede, 1973; Dries and Theede, 1974). Therefore, it appears likely that salinity fluctuations, low oxygen levels and more frequent anaerobiosis resulted in lower biomineralization rates in the ocean quahog and eventually the formation of numerous disturbance lines.

Both *Astarte* species seem to have coped better with the hostile environmental conditions, at least the biomineralization

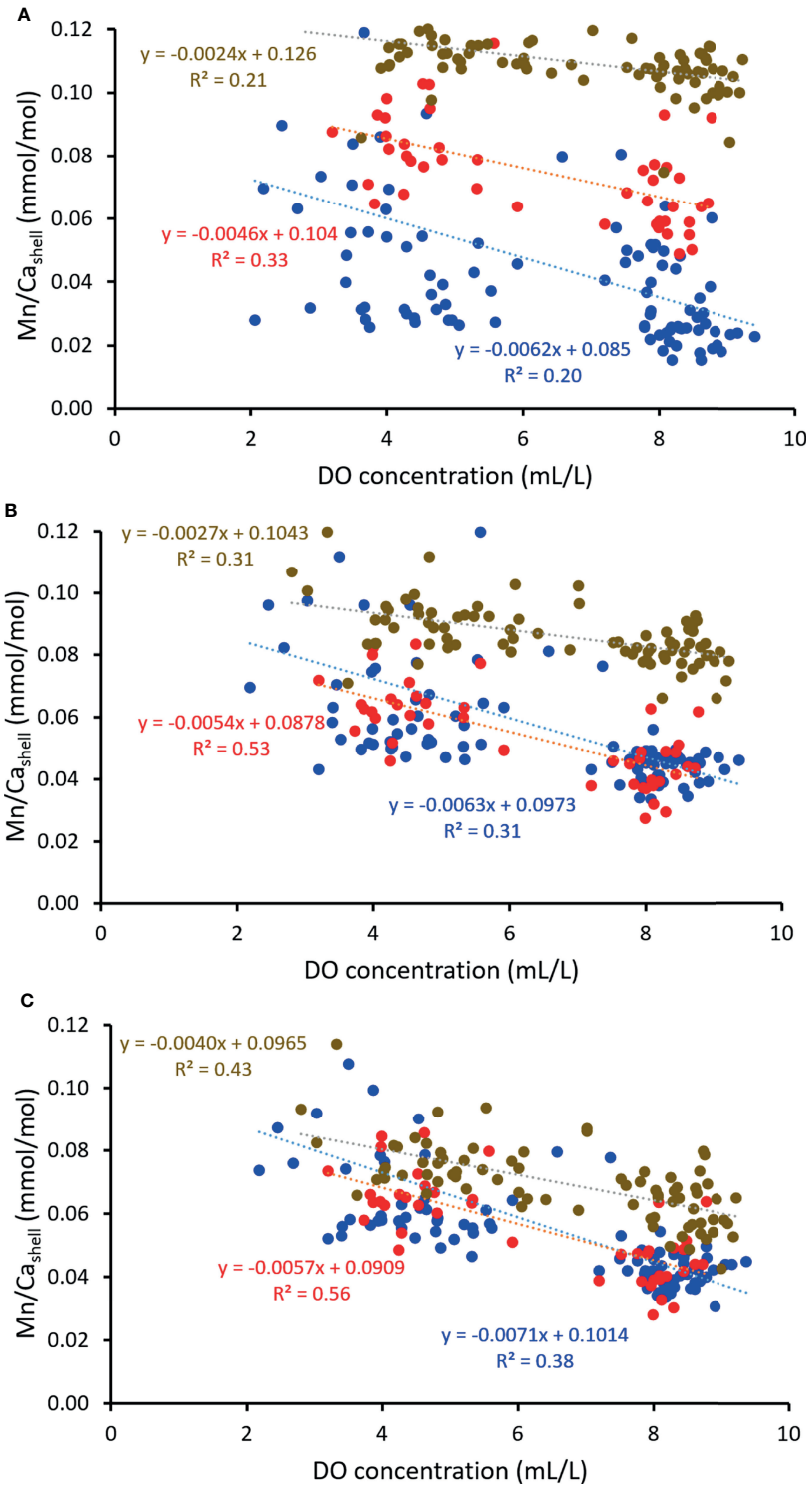

FIGURE 10 | Effect of different detrending techniques on the linear relationship between Mn/Ca_{shell} of bivalves dwelling at seafloor and DO concentration measured some decimeters above seafloor. All correlations were highly significant at $p < 0.0001$. **(A)** Ontogenetic age trends removed; **(B)** Annual growth rate-detrended and **(C)** double detrended data, i.e., correlation between Mn/Ca_{shell} with annual growth rate and Mg/Ca_{shell} mathematically eliminated. Blue = *A. islandica*; red = *A. elliptica*; brown = *A. borealis*.

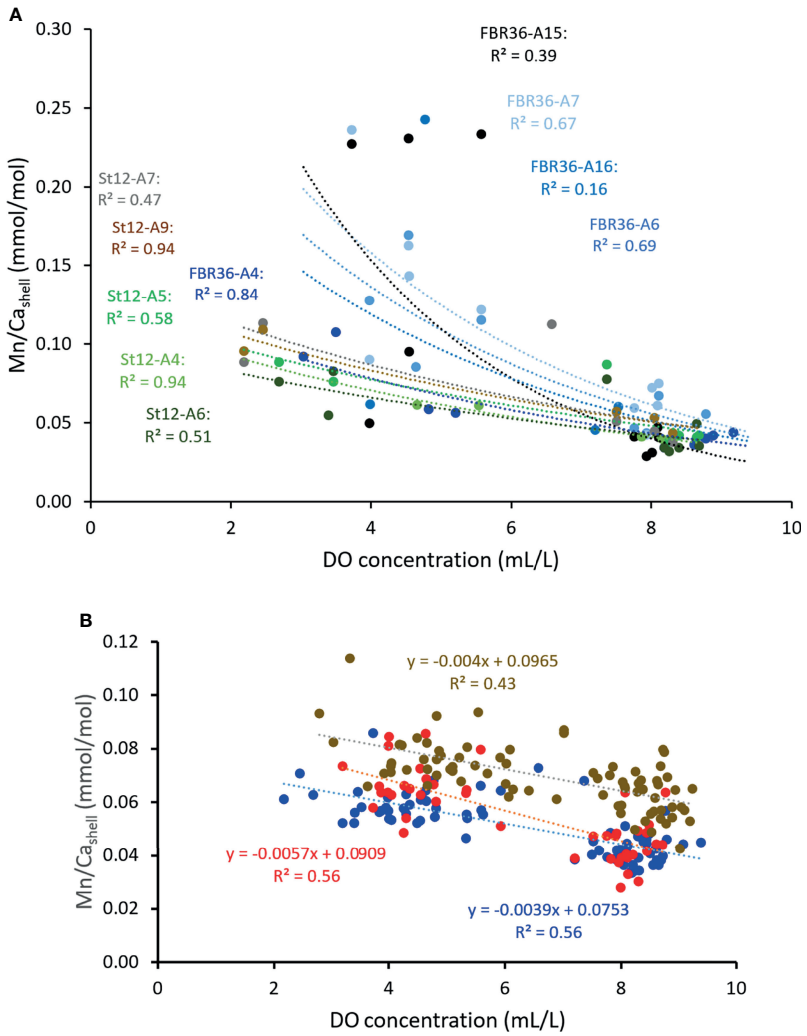

FIGURE 11 | **(A)** During early ontogeny (below age 10), Mn/Ca$_{shell}$ revealed non-linear relationships (here exponential fits used), even after double-detrending (= correlation between Mn/Ca$_{shell}$ with both annual growth rate and Mg/Ca$_{shell}$ mathematically eliminated). Significance levels were determined on the basis of linear regression models. Accordingly, except for specimens FBR36-A16 and St12-A7, all correlations were highly significant at $p < 0.05$. Trends varied between specimens, not localities. St12 = Mecklenburg Bight, FBR36 = Fehmarn Belt. **(B)** If the data from shell portions formed prior to age 10 were omitted, the relationship between Mn/Ca$_{shell}$ of *A. islandica* and DO concentration measured some decimeters above seafloor became much stronger. All correlations were highly significant at $p < 0.0001$. (Compare **Figure 10C**).

processes did not seem to have been impacted as much. The shells were thick (see also Oeschger, 1990; Rumohr and Krost, 1991) and the inner shell layers fully developed without signs of significant dissolution. Judging from fewer disturbance lines, the biomineralization process was also less frequently interrupted. Thus, their shells may provide a more reliable and more complete record of the ocean oxygenation than the ocean quahog. The recognition of annual growth lines was much easier in the astartids, specifically in *A. elliptica*. Besides the presence of blue-stained annual bands and lines after immersion in Mutvei's solution, sharp Mg/Ca$_{shell}$ peaks and troughs aided in the identification of the annual growth lines in this species. Note that these Mg (as well as Sr) enrichments did not coincide with the coldest or warmest season suggesting that Mg and Sr were not primarily governed by temperature.

While *A. elliptica* can provide slightly more precise DO estimates than the other two species (**Figure 12**), the disadvantage is its relatively short lifespan of only twenty years or so (**Table 1**). Furthermore, strong undulations of the outer shell layer that mirrored spiral ridges of the outer shell surface (**Figure 2B**), made sampling a challenging task and often resulted in strongly time-averaged chemical data. Such difficulties were not encountered in *A. borealis* (**Figure 2C**). This species only showed a weak wavy sculpture that barely affected the geometry of growth patterns in the outer shell layer. *A. borealis* attained the longest lifespan of the studied species

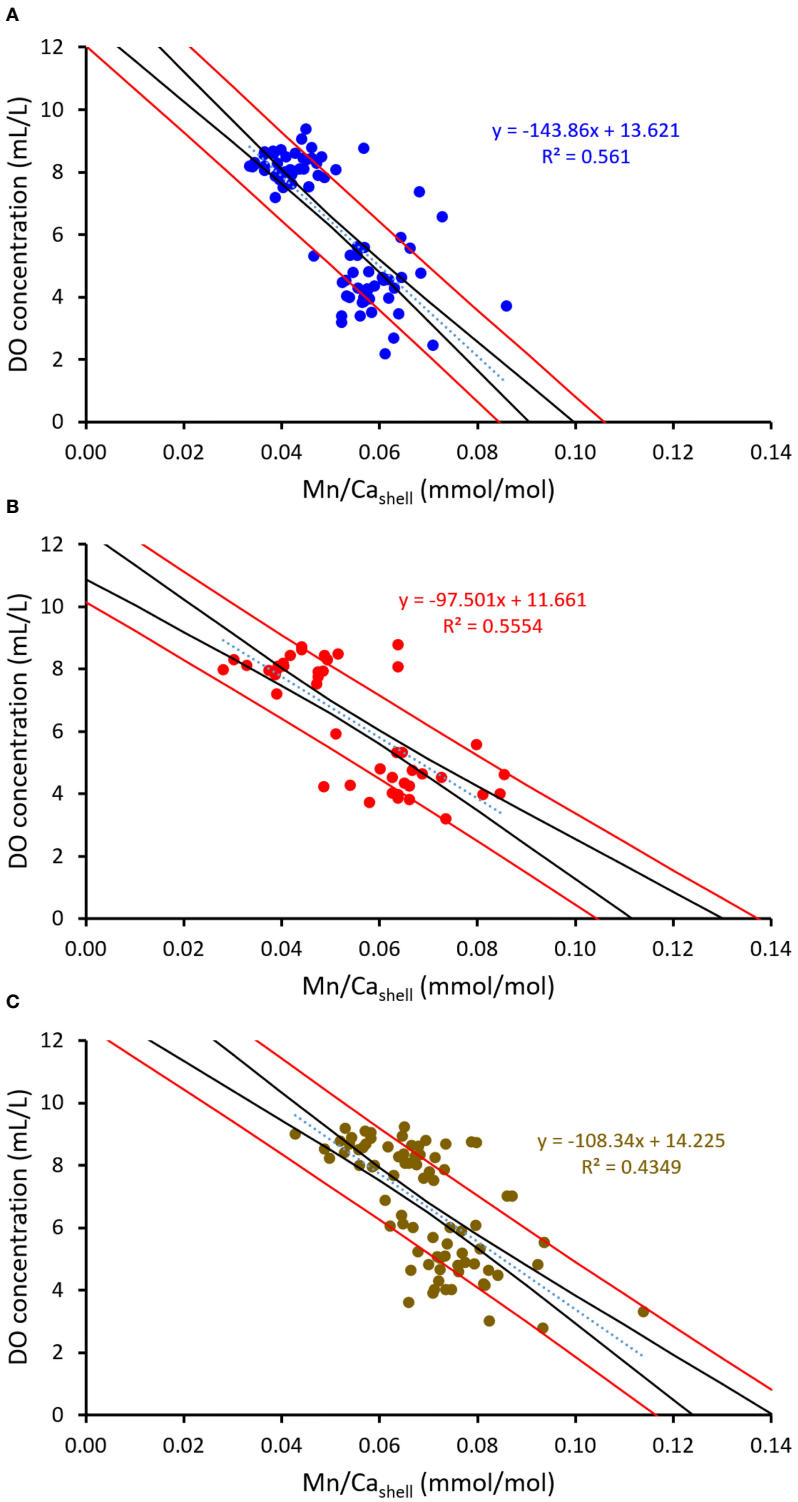

FIGURE 12 | Tentative linear models to predict DO concentration some decimeters above seafloor using Mn/Ca$_{shell}$ values of the three studied bivalve species (N = 79 **(A)**, 44 **(B)** and 80 **(C)**; all $p < 0.0001$). **(A)** *A. islandica*; **(B)** *A. elliptica*; **(C)** *A. borealis*. Black curves = 95% confidence intervals of the regression lines; red curves = 1σ prediction intervals. *A. elliptica* can provide slightly more precise DO data (± 1.5 mL/L) than *A. islandica* or *A. borealis* (± 1.6 mL/L).

(**Table 1**), which is an important prerequisite to assess the long-term trends or quasi-decadal cycles of ocean ventilation.

If the advantages and disadvantages of the studied species are weighed up against each other and more than a single species is available for DO reconstructions, preference should be given to the two *Astarte* species, because the growth patterns are easier to identify than in the ocean quahog facilitating the temporal alignment of the LA spots. Since the shell formation remained largely unimpeded by salinity and low oxygen stress, the studied astartids offer better chances to record the most extreme deoxygenation events. If the most precise DO estimates are needed, *A. elliptica* should be given preference, whereas long-term trends may be easiest obtained from *A. borealis*. Mn/Ca_{shell} data of *A. islandica* and *A. elliptica* may be combined to infer DO levels, because the transfer functions of both species were nearly identical (**Figures 12B, C**; **Supplements**).

4.2 Mn/Ca_{shell} Serve as a Proxy for DO Levels in the Water Column

The covariation between detrended Mn/Ca_{shell} and DO concentration suggests that the primary source for this metal in the shell was dissolved Mn^{2+}, i.e., hydrated ions, complexes or colloids rather than particulate Mn. The strongest Mn enrichment was observed in shell portions formed between July and September, i.e., contemporaneously with the lowest oxygen levels in the water column, but several months after the primary production maximum and associated downward flux of Mn-rich organic particles, and several months before the halocline disrupted giving way to increased bottom currents that may have stirred up Mn-bearing particles from the sea floor. Sharp Mn/Ca_{shell} peaks as previously reported from *A. islandica* of Mecklenburg Bight (Schöne et al., 2021) could potentially be derived from digested particulate Mn. However, the seasonal Mn/Ca_{shell} oscillations that covary with DO support a predominant dissolved source of this metal. Controlled laboratory experiments in future studies would certainly be useful to shed light on the relative importance of the different Mn sources.

In-situ analyses would also be useful to clarify the degree to which the incorporation of this metal into the shell is controlled by biological effects and whether equilibrium with Mn^{2+} in the ambient water is attained at some stage of life. As the concentration of Mn^{2+} (as well as DO) at the very position where the food intake takes place is unknown (note again, in the present study and in Schöne et al., 2021, Mn/Ca_{shell} values were compared to DO concentration some decimeters above the seafloor), not even a rough estimate on the magnitude of the vital effects and its change through lifetime is possible. With their extremely short siphons (e.g., Morton, 2011), the studied endobenthic bivalves inhaled water directly from the sediment-water interface, i.e., where dissolved Mn diffuses out of the sediment (Sundby et al., 1981; Roitz et al., 2002) and mixes with the overlaying water body. The highest Mn^{2+} concentrations (and lowest DO levels) within the water column occur just here, at the sediment-water interface and gradually decline with increasing distance from the sediment surface while DO levels rise (e.g., Kremling and Petersen, 1978). At least, the strong correlation between detrended Mn/Ca_{shell} values recorded at the seafloor and DO levels measured some decimeters away from the sediment surface suggests that the Mn^{2+} concentrations and DO levels in the water column changed proportionately to that in the fluffy layer at the seabed which has important implications for the use of this proxy. Subsequent studies should evaluate if and how strongly the relationship of DO (and Mn/Ca) within the coelomic fluid of the bivalves (containing inhaled water), directly at the sediment-water interface and different heights above the seafloor varies over time. With such knowledge, it may also be possible to further constrain the relationship between DO and Mn/Ca_{shell} values. Furthermore, if the relationship between DO within the coelomic fluid and at various heights above seafloor is known, it may also become possible to estimate bottom DO concentrations from Mn/Ca_{shell} values.

The concentration of dissolved manganese near the sediment-water interface typically can vary among localities, depending on DO level, duration of oxygen deficiency, amount of Mn-rich particles at the sea floor, bottom currents etc. (Limburg et al., 2011). For example, Groeneveld et al. (2018) reported water column Mn/Ca values of approx. 5 μmol/mol at 5 mL/L DO and above, and more than 200 μmol/mol at 2 mL/L DO at Hanö Bay. However, in the Kattegat, $Mn/Ca_{seawater}$ values remained below 23 μmol/mol even near the normoxic/hypoxic boundary (Groeneveld et al., 2018). In the present study, the DO vs. Mn/Ca_{shell} data from Mecklenburg Bight and Fehmarn Belt fitted very well to each other (and were thus combined in the same prediction model) suggesting similar Mn fluxes into the water column. Subfossil shells from the same region should thus provide reasonable estimates on past DO levels in the water column some decimeters above seafloor.

Porewater Mn^{2+} may have reached the site of biomineralization also through the mantle epithelia and foot. When gaping, a small portion of the mantle is constantly engulfed by porewater. In addition, when the animal digs into the sediment, the foot comes into contact with porewater. Hence, there were chances for diffusive transmembrane ion transport from the porewater into the blood and eventually the calcifying fluid or gel in the extrapallial space. However, the amounts of ions reaching the internal fluids through intercellular diffusion are small relative to active transmembrane ion transport (Carré et al., 2006) and most certainly remain far below the ion supply from the water column considering filtration rates, e.g., up to 7 L/h in the ocean quahog (Winter, 1969). The large amounts of water passing through the mantle coelom will likely dilute and remove most of the ions that arrived *via* diffusion from porewater before they can reach the extrapallial space.

Furthermore, the strong correlation between detrended Mn/Ca_{shell} and DO implies that the water inhaled through the siphons was the major contributor of Mn^{2+} (and other ions) in the shells rather than diffusion from porewater. In contrast to the water column, oxygen levels in the porewater likely did not vary notably on seasonal time-scales, specifically in the mud/fine-silt-dominated, organic-rich sediment in which *A. borealis* lived. Dissolved Mn concentrations in the porewater should thus have

remained nearly invariant over time and were very likely much higher than above the sediment surface. Furthermore, larger, ontogenetically older, deeper digging specimens would have been exposed to much higher Mn concentrations than younger specimens would, but the opposite was observed: The highest Mn concentrations were measured in shell portions formed during youth.

4.3 Controls on Mn Incorporation Into the Shells

Faster growing shell portions contained larger amounts of manganese than slower growing shell portions (**Figures 8A–C**). Similar trends have previously been reported from two aragonitic shells from Peru, *Mesodesma donacium* and *Chione subrugosa*, and were ascribed to growth rate-related kinetic effects (Carré et al., 2006). At first sight, this finding indeed points to kinetic processes as it agrees well with results from synthetically precipitated aragonite (Kumagai, 1978). A possible explanation is that faster precipitation is associated with the coprecipitation of ions that would otherwise not fit into the orthorhombic crystal lattice of aragonite, e.g., monovalent ions (Rollion-Bard and Blamart, 2015) or divalent ions that are more than 15% larger or smaller than Ca^{2+} (114 pm) (Kretz, 1982) thereby resulting in a larger number of lattice defects (Amiel et al., 1973). Ba^{2+}, Mn^{2+} and Mg^{2+} belong to the latter group. The ion radius of high-spin Mn^{2+}, which is present in bivalve shell aragonite (Soldati et al., 2016; Son et al., 2019), measures 83 pm, Mg^{2+} 72 pm, and Ba^{2+} 147 pm (Speer, 1983). To accommodate Mn^{2+} in the crystal lattice of aragonite, local calcite coordination domains are generated so that Mn^{2+} is coordinated by a CO_3-octahedron (e.g., Soldati et al., 2016). The same process likely ensures that Mg^{2+} can be accommodated in the aragonitic crystal lattice.

Following this rationale, faster growing shell portions should not only contain more Mn^{2+}, but also larger amounts of Na^+, Li^+, K^+, Mg^{2+} etc., because these ions are present in the calcifying solution and nearly as highly concentrated as in the ambient seawater (e.g., Crenshaw, 1972; Wada and Fujinuki, 1976; Lorens and Bender, 1980). While the two Peruvian bivalves cited earlier fulfilled this expectation, and shell Sr/Ca, Ba/Ca, and Mg/Ca were positively coupled to growth rate as well (Carré et al., 2006), the opposite was found in the present study for Sr/Ca_{shell} and Mg/Ca_{shell}, specifically in old-grown specimens (**Figure 6**). These two element-to-Ca ratios were thus inversely correlated to Mn/Ca_{shell} suggesting vital effects played a more important role during Mn incorporation into the shell aragonite than processes prevailing in abiotic systems.

This interpretation is further supported, firstly, by the fact that many trace impurities in bivalve shells remain far below concentrations expected for equilibrium precipitation. For example, Mg/Ca_{shell} values in aragonitic bivalve shells such as *A. islandica* range between approx. 0.2 to 1.3 mmol/mol (Schöne et al., 2011; and data herein), whereas seawater contains 5.5 mol/mol. Based on experimentally determined distribution coefficients for Mg/Ca in synthetic aragonite provided by Gaetani and Cohen (2006), between 5°C and 15°C, the shells should contain approx. 81.95 to 9.35 mmol/mol. As no direct measurements of Mn/Ca values are available from the water near the seabed where the bivalves fed, no reliable conclusions can be drawn on the degree of a possible disequilibrium for this metal in shell aragonite. Secondly, lattice distortions can also be physiologically induced in biominerals by the insertion of proteins into the crystal lattice (Pokroy et al., 2006), perhaps as a response to manganese enrichment in the ambient water and the requirement for detoxification (see below). Thirdly, in abiogenic systems, interactions between ions in the calcifying solution can prevent the incorporation of some and favor the incorporation of other ions into the $CaCO_3$ crystal lattice (Okumura and Kitano, 1986; Dromgoole and Walter, 1990). For example, Mg^{2+} competes more successfully than Mn^{2+} for adsorption sites on growing crystal surfaces of calcite and suppresses the incorporation of Mn^{2+} into the crystal lattice (Dromgoole and Walter, 1990). Assuming the few reports on the chemistry of the extrapallial fluid or gel (Crenshaw, 1972; Wada and Fujinuki, 1976; Lorens and Bender, 1980) are correct and kinetics are the same as in pure calcite, the studied shells, more specifically the calcite domains in the aragonite should be almost devoid of Mn^{2+}. However, the opposite clearly is the case, pointing to a significant participation of vital effects during shell growth.

Whereas vital effects can result in much lower distribution coefficients than expected for thermodynamic equilibrium, trace elements such as Sr^{2+} are still incorporated into the shell proportional to that in the water (Zhao et al., 2017b). Based on the findings herein, this also applies to Mn^{2+}, a major prerequisite to employ this trace metal as a DO proxy in bivalves. The proportionate increase of Mn^{2+} in the shells may also reflect attempts to detoxify, i.e., to remove unwanted ions from the body fluids either by pumping them out of the mantle coelom or by using the shell as a recycle bin. Mn^{2+} is one these 'unwanted' ions, because it can be toxic for bivalves at elevated concentration as it interferes with neurotransmitters that control the beating of the cilia of the gills (Nelson et al., 2018).

After mathematical detrending for growth rate-related kinetic effects as well as vital effects that affected the incorporation of both Mg^{2+} and Mn^{2+} into the shell, the Mn/Ca_{shell} data agreed much better with DO (**Figure 10C**). However, during early ontogeny (< age 10), *A. islandica* shells still contained much larger amounts of Mn^{2+}, than during later stages of life, and large individual differences in juvenile Mn^{2+} enrichment were observed (**Figure 11A**). Possible reasons include microhabitat differences, e.g., variations in Mn flux from the seabed into the overlaying water body, or physiological differences among specimens. In addition, older specimens likely produced a much stronger current through their siphons and thus sucked in water farther away from the sediment-water interface where Mn^{2+} concentrations were lower than directly at the seabed, while young specimens with weaker muscles accessed a larger proportion of water from the fluffy layer. Individual fitness may account for differences in juvenile Mn^{2+} enrichment among specimens. Another possibility is that older specimens were more effective in removing unwanted ions from body fluids

including the site of biomineralization and thus contained lower amounts of Mn^{2+} than younger specimens. Some juveniles may have invested more energy into shell growth rather than a chemically cleaner shell. As in abiogenic aragonite, larger amounts of trace impurities, specifically Mg^{2+} can increase the hardness of the shells (Boon et al., 2019); presumably, the same applies to Mn^{2+}. However, at the same this makes them more amenable to fractures, because the shells become more brittle, less elastic. Yet, this disadvantage may outweigh the danger of being eaten by a predator due insufficient body size.

It remains unclear whether such Mn enrichment during youth also occurs in *Astarte* spp., because respective shells portions could hardly be sampled due to the peculiar growth pattern geometry and/or a thin outer shell layer in early ontogeny. Judging from the few data of specimens MLZ-FBR-A8 and A10 as well as MLZ-FBR06-A1 and A3, Mn^{2+} is not as strongly elevated in shells of young *Astarte* spp. than in the ocean quahog. Pending confirmation of this finding, astartids may be more efficient in excluding Mn from incorporation into the shell carbonate than the ocean quahog. Alternatively, they generate a stronger current through their siphons during youth than coeval specimens of *A. islandica* resulting in the uptake of water farther away from Mn-enriched fluffy layer.

The relationship between detrended Mn/Ca_{shell} values (above the age of ten) and DO levels in the water column varied only slightly between *A. islandica* and *A. elliptica* (**Figure 10C**) suggesting that largely similar mechanisms were at work during manganese uptake, transport and incorporation into the shell. However, *A. borealis* incorporated, on average, approx. 20 µmol/mol more manganese in its shell than the other two species (**Figure 10C**). These differences could reflect species-specific vital effects controlling the incorporation of trace impurities into the shell or site-specific differences in porewater Mn^{2+} fluxes, bottom currents etc. In light of similar transfer functions for co-occurring bivalves belonging to different genera, i.e., *A. islandica* and *A. elliptica*, site-specific differences in Mn availability do not seem unlikely to explain the higher level in *A. borealis*.

4.4 Detrending

The double-detrending approach eliminated a significant proportion of physiological and growth rate-related kinetic effects (**Figure 10C**), but was uncapable of removing the heteroscedastic noise from the Mn/Ca_{shell} chronologies of *A. islandica*, i.e., the decreasing Mn/Ca_{shell} amplitudes with increasing ontogenetic age and slower shell growth (**Figure 5A**). In dendrochronology and bivalve sclerochronology, annual growth rates typically exhibit a strong heteroscedasticity, which can be mathematically eliminated with an adaptive power transformation (Cook and Peters, 1997). Briefly, the local mean and variance of annual increment widths are linearly correlated when plotted in logarithmic space. A data-adaptive power transformation of these data can be used to normalize the raw data based on the slope of the regression line and produce variance-stabilized (= homoscedastic) growth data (see step-by-step explanation in Cook and Peters, 1997, and for application in sclerochronology see Schöne, 2013). A similar approach could theoretically be used to remove the heteroscedasticity from the Mn/Ca_{shell} chronologies provided they were at least as long as the that of specimen MLZ-FBR36-A4. This is because a broad spectrum of log mean vs. log variance pairs were needed for each specimen to obtain a robust regression line and slope for the variance correction. Notably, a data-adaptive power transformation can only be performed on individual chronologies, because the absolute changes of Mn/Ca_{shell} values during different ontogenetic ages in the same specimen must be known. As shown in **Figures 5A**, **7A**, **9A**, during early stages of life, studied specimens of *A. islandica* showed large differences in seasonal Mn/Ca_{shell} amplitudes making it impossible to predict how the Mn/Ca_{shell} curves would develop during subsequent years. Furthermore, due to strong individual differences in Mn/Ca_{shell} amplitudes of coeval specimens (**Figure 11A**), no common non-linear relationship exists between DO concentration and Mn/Ca data of shell portions produced until the age of ca. nine. Therefore, no reliable method currently exists to infer DO from shells of ontogenetically young specimens of *A. islandica*. Since the Mn/Ca_{shell} chronologies were largely homoscedastic from age ten onward (**Figure 5A**) and no variance correction was required, it seems justified to simply disregard the data from the first nine years of life in the prediction model for *A. islandica* (**Figure 12A**).

Growth rate-related kinetics demonstrably affected the Mn/Ca_{shell} data (**Figures 8A–C**). In the present study, removal of growth rate-related trends was exclusively accomplished on the basis of annual shell growth rates, i.e., (resampled) daily and monthly Mn/Ca_{shell} data were detrended with the annual growth value of the respective growing season. Ideally, daily growth rates should have been used to detrend Mn/Ca_{shell} data. However, daily increment width data were not available and the generalized seasonal growth model may not perfectly reflect the actual daily growth rates in each year. To avoid large errors resulting from the use of inappropriate (interpolated) daily growth data, the annual increment widths were used instead.

5 SUMMARY AND CONCLUSION

Manganese-to-Ca ratios in shells of all three studied bivalves from the Baltic Sea, *A. islandica*, *A. elliptica* and *A. borealis* can provide robust information (1σ error of ±1.5 to 1.6 mL/L) on the concentration of dissolved oxygen in the water column some decimeters above seafloor using species-specific transfer functions. Once the raw data were temporally contextualized with an appropriate seasonal age model and corrected for differences in time-averaging, the resampled Mn/Ca_{shell} chronologies require detrending, ideally the mathematical elimination of both the correlation with annual growth rate and Mg/Ca_{shell} values. This treatment removes a large proportion of vital (and potentially kinetic) effects. Due to specimen-specific non-linear relationships between DO and Mn/Ca_{shell} as well as

strong heteroscedasticity of Mn/Ca_{shell}, data from the first nine years of life of *A. islandica* should not be used for DO reconstructions. Findings of the present study provide the basis to reconstruct inter-annual trends of seasonal DO extremes in nearshore coastal environments of the Baltic Sea during the most recent centuries.

DATA AVAILABILITY STATEMENT

The original contributions presented in the study are included in the article/**Supplementary Material**. Further inquiries can be directed to the corresponding author.

AUTHOR CONTRIBUTIONS

BS: conceptualization, data curation, formal analysis, investigation, methodology, project administration, supervision, validation, visualization, writing – original draft preparation, writing – review and editing. XH: sample preparation, data curation, methodology, formal analysis. AJ: writing – review and editing. RM-K: resources, validation, writing – review and editing. MZ: resources, writing – review and editing. All authors contributed to the article and approved the submitted version.

FUNDING

This study was made possible by a German Research Foundation (DFG) grant to BRS (SCHO 793/22). The sampling cruise was financed as part of the LEGRA project funded by the Federal Agency for Nature Conservation (BfN) (FKZ 3519532202).

ACKNOWLEDGMENTS

We thank Lukas Fröhlich, Qian Huang, Katharina Schmitt, Thomas Tütken, Hao Wu and Michael Maus for fruitful discussions during analyses and interpretation of the data. Michael Maus is also gratefully acknowledged for his help with stable isotope analysis. We thank Dr. Alexander Darr for leading the research cruise. We also thank two reviewers for their thoughtful comments that helped to further improve the quality of the manuscript and increase its clarity.

SUPPLEMENTARY MATERIAL

The Supplementary Material for this article can be found online at: https://www.frontiersin.org/articles/10.3389/fmars.2022.820731/full#supplementary-material

REFERENCES

Abbott R. T., Morris P. A. (1995). *A Field Guide to Shells: Atlantic and Gulf Coasts and the West Indies* (Houghton Mifflin: New York), 512.

Amiel A. J., Friedman G. M., Miller D. S. (1973). Distribution and nature of trace elements in modern aragonitic corals. *Sedimentol.* 20, 47–64. doi: 10.1111/j.1365-3091.1973.tb01606.x

Arntz W. E., Weber W. (1970). *Cyprina islandica* L. (Mollusca, Bivalvia) Als Nahrung Von Dorsch Und Kliesche in Der Kieler Bucht. *Ber. Dt. Wiss. Komm.* 2, 193–209.

Arthur M. A., Sageman B. B. (1994). Marine black shales: depositional mechanisms and environments of ancient deposits. *Annu. Rev. Earth Planet. Sci.* 22, 499–551. doi: 10.1146/annurev.ea.22.050194.002435

Balzer W. (1982). On the distribution of iron and manganese at the sediment/water interface: Thermodynamic versus kinetic control. *Geochim. Cosmochim. Acta* 46, 1153–1161. doi: 10.1016/0016-7037(82)90001-1

Benson B. B., Krause D.Jr. (1984). The concentration and isotopic fractionation of oxygen dissolved in freshwater and seawater in equilibrium with the atmosphere. *Limnol. Oceanogr.* 29, 620–632. doi: 10.4319/lo.1984.29.3.0620

Black B. A., Andersson C., Butler P. G., Carroll M., DeLong K. L., Reynolds D. J., et al. (2019). The revolution in marine paleoecology and paleoclimatology. *Biol. Lett.* 15, 20180665. doi: 10.1098/rsbl.2018.0665

Boon M., Rickard W. D. A., Rohl A. L., Jones F. (2019). Stabilization of aragonite: Role of Mg^{2+} and other impurity ions. *Cryst. Growth Des.* 20, 5006–5017. doi: 10.1021/acs.cgd.0c00152

Branson O., Fehrenbacher J., Vetter L., Sadekov A. Y., Eggins S. M., Spero H. J. (2019). Latools: A data analysis package for the reproducible reduction of LA-ICPMS data. *Chem. Geol.* 504, 83–95. doi: 10.1016/j.chemgeo.2018.10.029

Bryan S. P., Marchitto T. M. (2008). Mg/Ca-temperature proxy in benthic foraminifera: New calibrations from the florida straits and a hypothesis regarding Mg/Li. *Paleoceanogr* 23, PA2220. doi: 10.1029/2007PA001553

Butler P. G., Wanamaker A. D.Jr., Scourse J. D., Richardson C. A., Reynolds D. J. (2013). Variability of marine climate on the north icelandic shelf in a 1357-year proxy archive based on growth increments in the bivalve *Arctica islandica*. . *Palaeogeogr Palaeoclimatol. Palaeoecol.* 373, 141–151. doi: 10.1016/j.palaeo.2012.01.016

Carré M., Bentaleb I., Bruguier O., Ordinola E., Barrett N. T., Fontugne M. (2006). Calcification rate influence on trace element concentrations in aragonitic bivalve shells: evidences and mechanisms. *Geochim. Cosmochim. Acta* 70, 4906–4920. doi: 10.1016/j.gca.2006.07.019

Carstensen J., Andersen J. H., Gustafsson B. G., Conley D. J. (2014). Deoxygenation of the baltic sea during the last century. *Prox. Nat. Acad. Sci.* 111, 5628–5633. doi: 10.1073/pnas.1323156111

Case D. H., Robinson L. F., Auro M. E., Gagnon A. C. (2010). Environmental and biological controls on Mg and Li in deep-sea scleractinian corals. *Earth Planet. Sci. Lett.* 300, 215–225. doi: 10.1016/j.epsl.2010.09.029

Conley D. J., Björck S., Bonsdorff E., Carstensen J., Destouni G., Gustafsson B. G., et al. (2009). Hypoxia-related processes in the baltic sea. *Environ. Sci. Technol.* 43, 3412–3420. doi: 10.1021/es802762a

Conley D. J., Carstensen J., Ærtebjerg G., Bondo Christensen P., Dalsgaard T., Hansen J. L. S., et al. (2007). Long-term changes and impact of hypoxia in danish coastal waters. *Ecol. Applicat.* 17, S165–S184. doi: 10.1890/05-0766.1

Cook E. R., Peters K. (1997). Calculating unbiased tree-ring indices for the study of climatic and environmental change. *Holocene* 7, 361–370. doi: 10.1177/095968369700700314

Crenshaw M. A. (1972). Inorganic composition of molluscan extrapallial fluid. *Biol. Bull.* 143, 506–512. doi: 10.2307/1540180

Crenshaw M. A. (1980). "Mechanisms of Shell Formation and Dissolution," in *Skeletal Growth of Aquatic Organisms: Biological Records of Environmental Change*. Eds. D. C. Rhoads and R. A. Lutz (New York: Plenum Press), p. 115–132.

Danz R., Gretscher P. (2004). C–DIC: A new microscopy method for rational study of phase structures in incident light arrangement. *Thin Solid Films* 462–463, 257–262. doi: 10.1016/j.tsf.2004.05.124

Darr A., Gogina M., Zetler M. L. (2014). Detecting hot-spots of bivalve biomass in the south-western baltic sea. *J. Mar. Syst.* 134, 69–80. doi: 10.1016/j.jmarsys.2014.03.003

Dries R. R., Theede H. (1974). Sauerstoffmangelresistenz mariner bodenvertebralen aus der westlichen ostsee. *Mar. Biol.* 25, 327–333. doi: 10.1007/BF00404975

Dromgoole E. L., Walter L. M. (1990). Inhibition of calcite growth rates by Mn2+ in $CaCl_2$ solutions at 10, 25, and 50°C. *Geochim. Cosmochim. Acta* 54, 2991–3000. doi: 10.1016/0016-7037(90)90116-3

Fennel K., Testa J. M. (2019). Biogeochemical controls on coastal hypoxia. *Annu. Rev. Mar. Sci.* 11, 105–130. doi: 10.1146/annurev-marine-010318-095138

Füllenbach C. S., Schöne B. R., Mertz-Kraus R. (2015). Strontium/lithium ratio in aragonitic shells of *Cerastoderma edule* (Bivalvia) – a new potential temperature proxy for brackish environments. *Chem. Geol.* 417, 341–355. doi: 10.1016/j.chemgeo.2015.10.030

Gaetani G. A., Cohen A. L. (2006). Element partitioning during precipitation of aragonite from seawater: A framework for understanding paleoproxies. *Geochim. Cosmochim. Acta* 70, 4617–4634. doi: 10.1016/j.gca.2006.07.008

Gillikin D. P., Dehairs F., Lorrain A., Steenmans D., Baeyens W., André L. (2006). Barium uptake into the shells of the common mussel (*Mytilus Edulis*) and the potential for estuarine paleo-chemistry reconstruction. *Geochim. Cosmochim. Acta* 70, 395–407. doi: 10.1016/j.gca.2005.09.015

Gonfiantini R., Stichler W., Rozanski K. (1995). *Standards and Intercomparison Materials Distributed by the International Atomic Energy Agency for Stable Isotope Measurements (IAEA-TECDOC-825)* (Vienna, Austria: International Atomic Energy Agency (IAEA). Available at: https://www-pub.iaea.org/MTCD/publications/PDF/te_825_prn.pdf (Accessed last access: 1 Nov. 2022).

Groeneveld J., Filipsson H. L. (2013). Mg/Ca and Mn/Ca ratios in benthic foraminifera: The potential to reconstruct past variations in temperature and hypoxia in shelf regions. *Biogeosci.* 10, 5125–5138. doi: 10.5194/bg-10-5125-2013

Groeneveld J., Filipsson H. L., Austin W. E. N., Darling K., McCarthy D., Krupinski N. B. Q., et al. (2018). Assessing proxy signatures of temperature, salinity, and hypoxia in the baltic sea through foraminifera-based geochemistry and faunal assemblages. *J. Micropalaeontol.* 37, 403–429. doi: 10.5194/jm-37-403-2018

Grossman E. L., Ku T.-L. (1986). Oxygen and carbon isotope fractionation in biogenic aragonite; temperature effects, chem. *Geol. Isot. Geosci. Sect.* 59, 59–74. doi: 10.1016/0168-9622(86)90057-6

Hallmann N., Schöne B. R., Irvine G. V., Burchell M., Cokelet E. D., Hilton M. (2011). An improved understanding of the alaska coastal current: the application of a bivalve growth-temperature model to reconstruct freshwater-influenced paleoenvironments. *Palaios* 26, 346–363. doi: 10.1080/15564894.2013.787566

Hausmann N., Robson H. K., Hunt C. (2019). Annual growth patterns and interspecimen variability in Mg/Ca records of archaeological *Ostrea edulis* (European Oyster) from the late mesolithic site of conors island. *Open Quat.* 5, 9. doi: 10.5334/oq.59

Hem J. D. (1963). Chemical equilibria and rates of manganese oxidation. *U.S. Geol. Surv. Water Supply Pap.* 1667-A, A1–A64. doi: 10.3133/wsp1667A

Herreid C. F.II (1980). Hypoxia in invertebrates. *Comp. Biochem. Physiol.* 67A, 311–320. doi: 10.1016/S0300-9629(80)80002-8

Jochum K. P., Nohl U., Herwig K., Lammel E., Stoll B., Hofmann A. W. (2005). GeoReM: A new geochemical database for reference materials and isotopic standards. *Geostand. Geoanal. Res.* 29, 333–338. doi: 10.1111/j.1751–908X.2005.tb00904.x

Jochum K. P., Weis U., Stoll B., Kuzmin D., Yang Q., Raczek I., et al. (2011). Determination of reference values for NIST SRM 610–617 glasses following ISO guidelines. *Geostand. Geoanal. Res.* 35, 397–429. doi: 10.1111/j.1751–908X.2011.00120.x

Jokinen S. A., Virtasalo J. J., Jilbert T., Kaiser J., Dellwig O., Arz H. W., et al. (2018). A 1500-year multiproxy record of coastal hypoxia from the northern baltic sea indicates unprecedented deoxygenation over the 20th century. *Biogeosci* 15, 3975–4001. doi: 10.5194/bg-15-3975-2018

Jones D. S. (1980). Annual cycle of shell growth increment formation in two continental shelf bivalves and its paleoecologic significance. *Paleobiology* 6, 331–340. doi: 10.1017/S0094837300006837

Jones D. S., Quitmyer I. R. (1996). Marking time with bivalve shells: oxygen isotopes and season of annual increment formation. *Palaios* 11, 340–346. doi: 10.2307/3515244

Kremling K., Petersen H. (1978). The distribution of Mn, Fe, Zn, Cd and Cu in baltic seawater; a study on the basis of one anchor station. *Mar. Chem.* 6, 155–170. doi: 10.1016/0304-4203(78)90025-7

Kretz R. (1982). A model for the distribution of trace elements between calcite and dolomite. *Geochim. Cosmochim. Acta* 46, 1979–1981. doi: 10.1016/0016-7037(82)90137-5

Kubota K., Shirai K., Murakami-Sugihara N., Seike K., Hori M., Tanabe K. (2017). Annual shell growth pattern of the stimpson's hard clam *Mercenaria stimpsoni* as revealed by sclerochronological and oxygen stable isotope measurements. *Palaeogeogr. Palaeoclimatol. Palaeoecol.* 465, 307–315. doi: 10.1016/j.palaeo.2016.05.016

Kumagai T. (1978). Coprecipitation of manganese with calcium carbonate. *Bull. Inst. Chem. Res. Kyoto Univ.* 56, 280–285.

Limburg K. E., Olson C., Walther Y., Dale D., Slomp C. P., Høie H. (2011). Tracking baltic hypoxia and cod migration over millennia with natural tags. *Proc. Nat. Acad. Sci.* 108, E177–E182. doi: 10.1073/pnas.1100684108

Lorens R. B., Bender M. L. (1980). The impact of solution chemistry on *Mytilus edulis* calcite and aragonite. *Geochim Cosmochim Acta* 44, 1265–1278. doi: 10.1016/0016-7037(80)90087-3

Marali S., Schöne B. R., Mertz-Kraus R., Griffin S. M., Wanamaker A. D.Jr., Butler P. G., et al. (2017a). Reproducibility of trace element variations (Na/Ca, Mg/Ca, Mn/Ca, Sr/Ca, and Ba/Ca) within and between specimens of the bivalve *Arctica islandica* – a LA-ICP-MS line scan study. *Palaeogeogr. Palaeoclimatol. Palaeoecol.* 484, 109–128. doi: 10.1016/j.palaeo.2016.11.024

Marali S., Schöne B. R., Mertz-Kraus R., Griffin S. M., Wanamaker A. D. Jr., Matras U., et al. (2017b). Ba/Ca ratios in shells of *Arctica islandica* – potential environmental proxy and crossdating tool. *Palaeogeogr. Palaeoclimatol. Palaeoecol.* 465, 347–361. doi: 10.1016/j.palaeo.2015.12.018

Morton B. (2011). The biology and functional morphology of *Arctica islandica* (Bivalvia: Arcticidae): A gerontophilic living fossil. *Mar. Biol. Res.* 7, 540–553. doi: 10.1080/17451000.2010.535833

Moss D. K., Surge D., Zettler M. L., Orland I. J., Burnette A., Fancher A. (2021). Age and growth of astarte borealis (Bivalvia) from the southwestern baltic sea using secondary ion mass spectrometry. *Mar. Biol.* 168, 133. doi: 10.1007/s00227-021-03935-7

Nelson M., Adams T., Ojo C., Carroll M. A., Catapane E. J. (2018). Manganese toxicity is targeting an early step in the dopamine signal transduction pathway that controls lateral cilia activity in the bivalve mollusc *Crassostrea virginica*. *Comp. Biochem. Physiol. C Toxicol. Pharmacol.* 213, 1–6. doi: 10.1016/j.cbpc.2018.07.002

Oeschger R. (1990). Long-term anaerobiosis in sublittoral marine invertebrates from the western baltic sea: *Halicryptus spinulosus* (Priapulida), *Astarte borealis* and *Arctica islandica* (Bivalvia). *Mar. Ecol. Prog. Ser.* 59, 133–143. doi: 10.1016/0022-0981(93)90153-F

Oeschger R., Storey K. B. (1993). Impact of anoxia and hydrogen sulphide on the metabolism of *Arctica isiandica* L. (Bivalvia). *J. Exp. Mar. Biol. Ecol.* 170, 213–226. doi: 10.1016/0022-0981(93)90153-F

Okumura M., Kitano Y. (1986). Coprecipitation of alkali metal ions with calcium carbonate. *Geochim. Cosmochim. Acta* 50, 49–58. doi: 10.1016/0016-7037(86)90047-5

Österblom H., Hansson S., Larsson U., Hjerne O., Wulff F., Elmgren R., et al. (2007). Human-induced trophic cascades and ecological regime shifts in the baltic sea. *Ecosyst.* 10, 877–889. doi: 10.1007/s10021-007-9069-0

Palacios R., Orensanz J. M., Armstrong D. A. (1994). Seasonal and lifelong variation of Sr/Ca ratio in shells of *Mya arenaria* from grays harbor (Washington) — An ancillary criterion in demographic studies. *Estuarine Coastal Shelf Sci.* 39, 313–327. doi: 10.1006/ecss.1994.1067

Peharda M., Walliser E. O., Markulin K., Purroy A., Uvanović H., Janekovic I., et al. (2019). *Glycymeris pilosa* (Bivalvia) – A high-potential geochemical archive of the environmental variability in the adriatic sea. *Mar. Environ. Res.* 150, 104759. doi: 10.1016/j.marenvres.2019.104759

Pokroy B., Fitch A. N., Lee P. L., Quintana J. P., Caspi E. N., Zolotoyabko E. (2006). Anisotropic lattice distortions in the mollusk-made aragonite: A widespread phenomenon. *J. Struct. Biol.* 153, 145–150. doi: 10.1016/j.jsb.2005.10.009

Rabalais N. N., Díaz R. J., Levin L. A., Turner R. E., Gilbert D., Zhang J. (2010). Dynamics and distribution of natural and human-caused hypoxia. *Biogeosci.* 7, 585–619. doi: 10.5194/bg-7-585-2010

Roitz J. S., Flegal A. R., Bruland K. W. (2002). The biogeochemical cycling of manganese in san francisco bay: temporal and spatial variations in surface water concentrations. *Estuar. Coast. Shelf Sci.* 54, 227–239. doi: 10.1006/ecss.2000.0839Sarthou

Rollion-Bard C., Blamart D. (2015). Possible controls on Li, Na, and Mg incorporation into aragonite coral skeletons. *Chem. Geol.* 396, 98–111. doi: 10.1016/j.chemgeo.2014.12.011

Rue E. L., Smith G. J., Cutter G. A., Bruland K. W. (1997). The response of trace element redox couples to suboxic conditions in the water column. *Deep-Sea Res. I* 44, 113–134. doi: 10.1016/S0967-0637(96)00088-X

Rumohr H., Krost P. (1991). Experimental evidence of damage to benthos by bottom trawling with special reference to *Actica islandica*. *Meeresforsch.* 33, 340–345.

Schöne B. R. (2008). The curse of physiology – challenges and opportunities in the interpretation of geochemical data from mollusk shells. *Geo-Mar. Lett.* 28, 269–285. doi: 10.1007/s00367-008-0114-6

Schöne B. R. (2013). *Arctica islandica* (Bivalvia): A unique paleoenvironmental archive of the northern north atlantic ocean. *Global Planet. Change* 111, 199–225. doi: 10.1016/j.gloplacha.2013.09.013

Schöne B. R., Dunca E., Fiebig J., Pfeiffer M. (2005a). Mutvei's solution: An ideal agent for resolving microgrowth structures of biogenic carbonates. *Palaeogeogr. Palaeoclimatol. Palaeoecol.* 228, 149–166. doi: 10.1016/j.palaeo.2005.03.054

Schöne B. R., Houk S. D., Freyre Castro A. D., Fiebig J., Kröncke I., Dreyer W., et al. (2005b). Daily growth rates in shells of *Arctica islandica*: Assessing subseasonal environmental controls on a long-lived bivalve mollusk. *Palaios* 20, 78–92. doi: 10.2110/palo.2003.p03-101

Schöne B. R., Huang X., Zettler M. L., Zhao L., Mertz-Kraus R., Jochum K. P., et al. (2021). Mn/Ca in shells of *Arctica Islandica* (Baltic Sea) – a potential proxy for ocean hypoxia? *Estuar. Coast. Shelf Sci.* 251, 107257. doi: 10.1016/j.ecss.2021.107257

Schöne B. R., Rodland D. L., Wehrmann A., Heidel B., Oschmann W., Zhang Z., et al. (2007). Combined sclerochronologic and oxygen isotope analysis of gastropod shells (*Gibbula cineraria*, North Sea): life-history traits and utility as a high-resolution environmental archive for kelp forests. *Mar. Biol.* 150, 1237–1252. doi: 10.1007/s00227-006-0435-9

Schöne B. R., Zhang Z., Radermacher P., Thébault J., Jacob D., Nunn E. V., et al. (2011). Sr/Ca and Mg/Ca ratios of ontogenetically old, long-lived bivalve shells (*Arctica islandica*) and their function as paleotemperature proxies. *Palaeogeogr. Palaeoclimatol. Palaeoecol.* 302, 52–64. doi: 10.1016/j.palaeo.2010.03.016

Shirai K., Schöne B. R., Miyaji T., Radermacher P., Krause R. A. Jr., Tanabe K. (2014). Assessment of the mechanism of elemental incorporation into bivalve shells (*Arctica islandica*) based on elemental distribution at the ultrastructural scale. *Geochim. Cosmochim. Acta* 126, 307–320. doi: 10.1016/j.gca.2013.10.050

Soldati A. L., Jacob D. E., Glatzel P., Swarbrick J. C., Geck J. (2016). Element substitution by living organisms: The case of manganese in mollusc shell aragonite. *Sci. Rep.* 6, 22514. doi: 10.1038/srep22514

Son S., Newton A. G., Lee J.-Y., Kwon K. D. (2019). Manganese speciation in Mn-rich $CaCO_3$: A density functional theory study. *Geochim. Cosmochim. Acta* 248, 231–341. doi: 10.1016/j.gca.2019.01.011

Speer J. A. (1983). Crystal chemistry and phase relations of orthorhombic carbonates. *Rev. Mineral* 11, 145–225. doi: 10.1515/9781501508134-009

Strahl J., Dringen R., Schmidt M. M., Hardenberg S., Abele D. (2011). Metabolic and physiological responses in tissues of the long-lived bivalve *Arctica islandica* to oxygen deficiency. *Comp. Biochem. Physiol.* A158, 513–519. doi: 10.1016/j.cbpa.2010.12.015

Sundby B., Silverberg N., Chesselet R. (1981). Pathways of manganese in an open estuarine system. *Geochim. Cosmochim. Acta* 45, 293–307. doi: 10.1016/0016-7037(81)90240-4

Taylor A. C. (1976). Burrowing activity and anaerobiosis of the bivalve *Arctica islandica* (L.). *J. Mar. Biol. Ass. U.K.* 56, 95–105. doi: 10.1017/S0025315400020464

Tebo B. M. (1991). Manganese(II) oxidation in the suboxic zone of the black sea. *Deep-Sea Res.* 38, Suppl. 2, S883–S905. doi: 10.1016/S0198-0149(10)80015-9

Theede H. (1973). Comparative studies on the influence of oxygen deficiency and hydrogen sulphide on marine bottom invertebrates. *Neth. J. Sea Res.* 7, 244–252. doi: 10.1016/0077-7579(73)90048-3

Theede H., Ponat A., Hiroki K., Schlieper C. (1969). Studies on the resistance of marine bottom invertebrates to oxygen-deficiency and hydrogen sulphide. *Mar. Biol.* 2, 325–337. doi: 10.1007/BF00355712

Trutschler K., Samtleben C. (1988). Shell growth of *Astarte elliptica* (Bivalvia) from kiel bay (Western Baltic Sea). *Mar. Ecol. Prog. Ser.* 42, 155–162. doi: 10.3354/meps042155

Tyson R. V., Pearson T. H. (1991). Modern and ancient continental shelf anoxia: An overview. *Geol. Soc Lond. Spec. Publ.* 58, 1–24. doi: 10.1144/GSL.SP.1991.058.01.01

Vaquer-Sunyer R., Duarte C. M. (2008). Thresholds of hypoxia for marine biodiversity. *Proc. Nat. Acad. Sci.* 105, 15453–15457. doi: 10.1073/pnas.0803833105

von Oertzen J.-A. (1973). Abiotic potency and physiological resistance of shallow and deep water bivalves. *Oikos* Suppl. 15, 261–266.

von Oertzen J.-A., Schlungbaum G. (1972). Experimentell-ökologische untersuchungen Über O_2-mangel- Und H_2S-resistenz an marinen evertebraten der westlichen ostsee. *Beitr. Meereskd.* 29, 79–91.

Wada K., Fujinuki T. (1976). "Biomineralization in Bivalve Molluscs with Emphasis on the Chemical Composition of the Extrapallial Fluid," in *The Mechanisms of Mineralization in the Invertebrates and Plants*. Eds. N. Watabe and K. M. Wilbur (Columbia, South Carolina, United States: Univ South Carolina Press), 175–190.

Wanamaker A. D.Jr., Gillikin D. P. (2019). Strontium, magnesium, and barium incorporation in aragonitic shells of juvenile *Arctica islandica*: Insights from temperature controlled experiments. *Chem. Geol.* 526, 117–129. doi: 10.1016/j.chemgeo.2018.02.012

Wanamaker A. D. Jr., Kreutz K. J., Wilson T., Borns H. W.Jr., Introne D. S., Feindel S. (2008). Experimentally determined Mg/Ca and Sr/Ca ratios in juvenile bivalve calcite for *Mytilus edulis*: Implications for paleotemperature reconstructions. *Geo-Mar. Lett.* 28, 359–368. doi: 10.1007/s00367-008-0112-8

Weigelt M., Rumohr H. (1986). Effects of wide range oxygen depletion on benthic fauna and demersal fish in kiel bay 1981-1983. *Meeresforsch.* 31, 124–136.

Winter J. E. (1969). Über den einfluß der nahrungskonzentration und anderer faktoren auf filtrierleistung und nahrungsausnutzung der muscheln *Arctica islandica* und *Modiolus modiolus*.. *Mar. Biol.* 4, 87–135. doi: 10.1007/BF00347037

Zettler M. L. (2001). Recent geographical distribution of the *Astarte borealis* species complex, its nomenclature and bibliography (Bivalvia: Astartidae). *Schr. Malakozool.* 8, 1–14.

Zettler M. L., Bönsch R., Gosselck F. (2001). Distribution, abundance, and some population characteristics of the ocean quahog, *Arctica islandica* (Linnaeus 1767) in the mecklenburg bight (Baltic Sea). *J. Shellf. Res.* 20, 161–169.

Zhao L., Schöne B. R., Mertz-Kraus R. (2017b). Controls on strontium and barium incorporation into freshwater bivalve shells (*Corbicula fluminea*). *Palaeogeogr. Palaeoclimatol. Palaeoecol.* 465, 386–394. doi: 10.1016/j.palaeo.2015.11.040

Zhao L., Walliser E. O., Mertz-Kraus R., Schöne B. R. (2017a). Unionid shells (*Hyriopsis cumingii*) record manganese cycling at the sediment-water interface in a shallow eutrophic lake in china (Lake Taihu). *Palaeogeogr. Palaeoclimatol. Palaeoecol.* 484, 97–108. doi: 10.1016/j.palaeo.2017.03.010

Conflict of Interest: The authors declare that the research was conducted in the absence of any commercial or financial relationships that could be construed as a potential conflict of interest.

Publisher's Note: All claims expressed in this article are solely those of the authors and do not necessarily represent those of their affiliated organizations, or those of the publisher, the editors and the reviewers. Any product that may be evaluated in this article, or claim that may be made by its manufacturer, is not guaranteed or endorsed by the publisher.